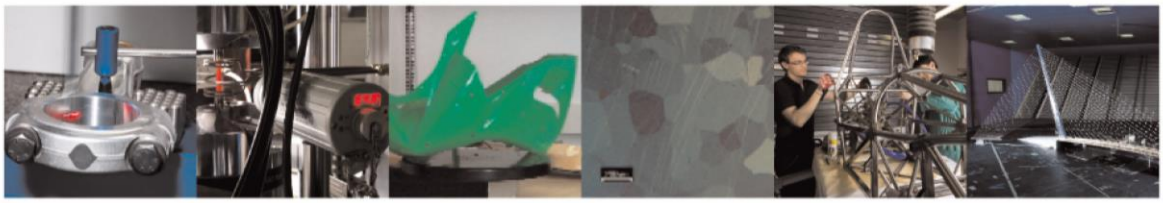

Process defects and in situ monitoring methods in metal powder bed fusion: A review

Grasso, MARCO LUIGI; Colosimo, BIANCA MARIA

This is a post-peer-review, pre-copyedit version of an article published in MEASUREMENT SCIENCE & TECHNOLOGY. The final authenticated version is available online at: http://dx.doi.org/10.1088/1361-6501/aa5c4f

DIPARTIMENTO DI MECCANICA ■ POLITECNICO DI MILANO
via G. La Masa, 1 ■ 20156 Milano ■ EMAIL (PEC): pecmecc@cert.polimi.it
http://www.mecc.polimi.it
Rev. 0

Process Defects and In-situ Monitoring Methods in Metal Powder Bed Fusion: a Review

Marco Grasso and Bianca Maria Colosimo

Dipartimento di Meccanica, Politecnico di Milano, Via La Masa 1, 20156
marcoluigi.grasso@polimi.it, biancamaria.colosimo@polimi.it

Abstract – Despite continuous technological enhancements of metal Additive Manufacturing (AM) systems, the lack of process repeatability and stability still represents a barrier for the industrial breakthrough. The most relevant metal AM applications currently involve industrial sectors (e.g., aerospace and bio-medical) where defects avoidance is fundamental. Because of this, there is the need to develop novel in-situ monitoring tools able to keep under control the stability of the process on a layer-by-layer basis, and to detect the onset of defects as soon as possible. On the one hand, AM systems must be equipped with in-situ sensing devices able to measure relevant quantities during the process, a.k.a. process signatures. On the other hand, in-process data analytics and statistical monitoring techniques are required to detect and localize the defects in an automated way. This paper reviews the literature and the commercial tools for in-situ monitoring of Powder Bed Fusion (PBF) processes. It explores the different categories of defects and their main causes, the most relevant process signatures and the in-situ sensing approaches proposed so far. Particular attention is devoted to the development of automated defect detection rules and the study of process control strategies, which represent two critical fields for the development of future smart PBF systems.

Keywords: Powder bed fusion (PBF), additive manufacturing (AM), selective laser melting (SLM), electron beam melting (EBM), in-situ sensing, in-process monitoring, process signature.

1. INTRODUCTION

In the recent years, metal additive manufacturing (AM) processes have been gaining a continuously increasing industrial attention for the production of functional components, ranging from one-of-a-kind to large scale productions. Additively produced parts exhibit innovative shapes, complex features and lightweight structures that are difficult or even impossible to produce with conventional processes. In this framework, ensuring the quality and repeatability of additively produced parts is a fundamental need to meet the stringent requirements and certification constraints imposed by leading sectors, like medical and aerospace. Nevertheless, the lack of process robustness, stability and repeatability was pointed out to be a major barrier for the industrial breakthrough of metal AM systems (Mani *et al*., 2015; Tapia and Elwany, 2014; Everton et al., 2016; Spear and Gold, 2016; Sharratt, 2015; Sames *et al*., 2016). Indeed, despite significant technological advances, the defect ratios are still too high with respect to more conventional production systems. To face this issue, the development of process monitoring methodologies based on in-situ sensing as well as novel feedback control strategies was indicated as a priority research area by many recent keynote studies, projects and roadmaps (Mellor et al., 2014; Olakanmi *et al*., 2015; Mani *et al*., 2015; Tapia and Elwany, 2014; Everton et al., 2016; Spear and Gold, 2016; Todorov *et al*., 2014). In-situ sensing and process monitoring are needed to determine the quality and stability of the process during the layer-wise growth of the part. Moreover, in-process data analytics allow one to make sense of the large amount of

acquired data and quickly detect the onset of defects and process errors. In addition, the defect avoidance implies the capability of adapting the process parameters based on in-situ measured quantities and, when possible, the implementation of closed-loop repairing actions. The research and development efforts related to these topics, pulled by urgent industrial needs, are becoming more intense and widespread every year, but the results are still far from the maturity reached in other manufacturing applications.

Recently, different review studies were devoted to defects and monitoring methods for metal AM processes. The studies of Sames *et al*. (2016) and Olakamni *et al*. (2015) and a report of the National Institute of Standard and Technology (NIST) (Mani *et al*., 2015) included a survey of metal AM processing defects. In addition, Tapia and Elwany (2014), Mani *et al*. (2015), Spears and Gold (2016) and Everton *et al*. (2016) presented a review of in-situ sensing and monitoring methods proposed in the literature. This study aims to contribute by merging a detailed discussion about the defect generation mechanisms with a review of the quantities that can be measured during the process and the corresponding in-situ sensing equipment. A classification of the state-of-the-art is presented with respect to different investigation fields and methodologies. Particular attention is devoted to data analysis and sensing techniques that allow an automated detection of the defects and, when possible, a reactive or corrective action. This review is focused on Powder Bed Fusion (PBF) processes, a metal AM category including Selective Laser Melting (SLM) and Electron Beam Melting (EBM). PBF systems allow higher feature resolution and accuracy with respect to other metal AM processes, at the expense of deposition rates and maximum build dimensions (Gibson *et al*., 2010). This makes the PBF technology suitable for precision metal AM applications, where avoidance of defects, discontinuities and inaccuracy is of critical importance. First, a review of the different kinds of defects that can occur during SLM and EBM processes is presented, together with a survey of their possible sources. Indeed, the comprehension of the nature and root causes of defects is fundamental to acquire a deeper knowledge of requirements, problems and challenges related to the design of process monitoring and control tools. Then, the different in-situ sensing approaches are discussed and compared, including already tested set-ups and novel sensors that are likely to be implemented in the future. The reviewed literature is mapped with respect to different measured quantities, a.k.a. process signatures, and different sensing solutions. Particular attention was devoted to the studies where automated defect detection rules and/or process control strategies were proposed and demonstrated. These latter studies still represent a small portion of the overall literature. This is related to many challenges that deserve further research efforts, e.g., the management of large amounts of data, the high sampling frequency needed to capture fast process dynamics, the lack of training samples in the presence of one-of-a-kind and highly customized products, the closed nature of most commercially available PBF system controllers[1], etc.

[1] Nevertheless, it is worth noting that there are efforts to develop an "Open Communication Protocol" for open communications of real-time, position-synchronized sensor data for PBF systems (Dunbar *et al*., 2016)

Section 2 reviews the possible defects and their causes in PBF; Section 3 reviews the literature of in-situ sensing and process monitoring; Section 4 reviews the studies and commercial tools devoted to automated in-process defect detection and control. Section 5 concludes the paper.

2. CATEGORIES OF DEFECTS AND THEIR CAUSES

2.1. The Powder Bed Fusion process

According to the standard ISO/ASTM 52900:2015, PBF is one of process category suitable for metal AM (ISO/ASTM 52900:2015(E)). PBF processes exploit a thermal energy source that selectively sinters (i.e., without melting to the point of liquefaction) or fuses regions of a thin powder layer. Selective laser sintering (SLS) was the first commercialized PBF process for metals. Later on, the technological enhancement of PBF systems and their power sources enabled the additive production of metal parts by fully melting the powder. In the melting process, a sufficient energy is provided to heat the material within a small region, referred to as the "melt pool", above the melting temperature. This enables production of components with better mechanical performances and properties than sintering methods. Currently, PBF processes (see Fig. 1) comprise **Selective Laser Melting (SLM)**, where the power source is a laser, and **Electron Beam Melting (EBM)**, where the power source is a high-energy electron beam. In both SLM and EBM, a thin layer of metal powder (e.g., typical prescribed thickness ranging between 30 - 50 µm) is deposited on a flat substrate via a powder deposition system (a.k.a. recoater). Then a galvanometer scanner (SLM) or a deflection coil (EBM) is used to displace the beam along a predefined path and to locally melt the powder to realize the first slice of the part. When the scan of the first layer is complete, the substrate is lowered, a new layer of powder is deposited and the process is repeated to realize the following slice (Gibson *et al.*, 2010). In SLM, the process takes place in an inert atmosphere (usually using nitrogen or argon) to avoid the formation of surface oxides during the layer-wise growth of the part. In EBM, the process takes place under a very low helium pressure (10^{-2} mbar) and at elevated temperatures. The low pressure He-atmosphere results in low impurity concentrations and allows processing reactive metal powders.

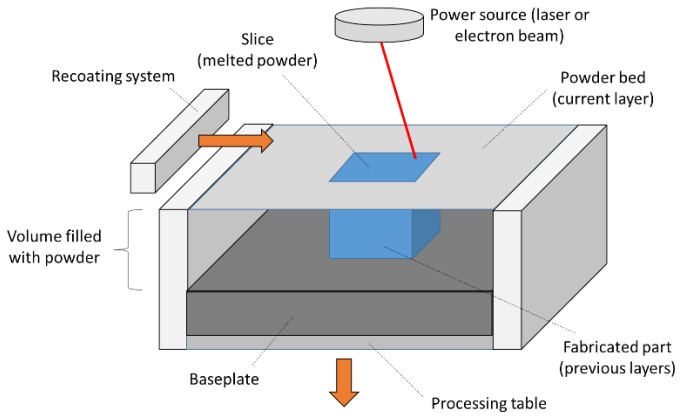

Fig. 1 – Scheme of PBF system (building chamber)

Table 1 – A mapping of main defects and their main causes discussed in the PBF literature

Sources of defects		Categories of defects					
		Porosity	**Balling**	**Geometric defects**	**Surface defects**	**Residual stresses, cracks & delamination**	**Microstructural inhomog. & impurity**
Equipment	**Beam scanning/ deflection system**	Foster et al., 2015		Moylan et al., 2014b; Foster et al., 2015			
	Build chamber environmental control	Ferrar et al., 2012; Spears and Gold, 2016	Li et al., 2012			Edwards et al., 2013; Chlebus et al., 2011; Buchbinder et al., 2014; Kempen et al., 2013	Spears and Gold, 2016
	Powder handling & deposition system	Foster et al., 2015		Foster et al., 2015; Kleszczynski et al., 2012	Foster et al., 2015; Kleszczynski et al., 2012		Foster et al., 2015
	Baseplate			Prabhakar et al., 2015		Prabhakar et al., 2015	
Process	**Parameters and scan strategy**	Matthews et al., 2016; Yasa et al., 2009; Attar, 2011; Gong, 2013; Read et al., 2015; Kruth et al., 2004; Weingarten et al., 2015; Thijs et al., 2010; Scharowsky et al., 2015; Puebla et al., 2012; Tammas-Williams et al., 2015; Biamino et al., 2011; Zeng, 2015	Li et al., 2012; Kruth et al., 2004; Tolochko et al., 2004; Zhou et al., 2015; Attar, 2011; Gong, 2013	Yasa et al., 2009; Mousa, 2016; Kleszczynski et al., 2012; Thomas, 2009	Li et al., 2012; Kruth et al., 2004; Matthews et al., 2016; Attar, 2011; Gong, 2013; Zaeh and Kanhert, 2009; Delgado et al., 2012;	Mercelis and Kruth, 2006; Parry et al., 2016; Cheng et al., 2016; Van Belle et al., 2013; Casavola et al., 2008; Zah and Lutzmann, 2010; Zaeh and Branner, 2010; Kempen et al., 2013; Kruth et al., 2004; Carter et al., 2012 - 2014	Carter et al., 2012 - 2014; Arisoy et al., 2016; Niu and Chang, 1999; Huang et al., 2016; Thijs et al., 2010; Scharowsky et al., 2015; Puebla et al., 2012; Biamino et al., 2011
	Byproducts and material ejections	Liu et al., 2015; Khairallah et al., 2016;					Liu et al., 2015; Khairallah et al., 2016;
Design for additive choices	**Supports**			Foster et al., 2015; Kleszczynski et al., 2012; Zeng, 2015	Foster et al., 2015; Kleszczynski et al., 2012; Zeng, 2015	Foster et al., 2015; Kleszczynski et al., 2012; Zeng, 2015	
	Orientation		Li et al., 2012; Strano et al., 2013;	Delgado et al., 2012	Delgado et al., 2012; Fox et al., 2016; Strano et al., 2013		Meier and Haberland, 2008
Feedstock material (powder)		Liu et al., 2015; Van Elsen, 2007; Das, 2003		Das, 2003	Seyda et al., 2012		Das, 2003; Niu and Chang, 1999; Huang et al., 2016

Different defects may originate during the process. Although, in some cases, post-processing techniques are suitable to mitigate or remove defects from PBF-produced parts (e.g., hipping), improving the quality of the as-build parts is fundamental to meet stringent and challenging industrial requirements. Understanding the defects and their causes represents the first step to design process monitoring and control tools. The different types of defects are first introduced and defined in subsection 2.2, and a review of their main causes is presented in subsection 2.3. The PBF literature devoted to defect characterization is mapped with respect to the defect category and the defect source in Table 1.

2.2. Categories of defects

2.2.1. Porosity

Porosity is particularly critical for most metal AM applications because it strongly impacts the fatigue performances and the crack growth characteristics of the part (Edwards *et al*., 2013). Because of this, porosity has been widely investigated in PBF (e.g., in Gu *et al*., 2013; Slotwinski et al., 2014; Weingarten et al., 2015). It consists of voids inside the bulk of the fused material. Those voids can be found i) within the layer part, ii) between adjacent layers, and/or iii) on the external surface of the part. More common pores are found within the layer, and they may have different size, shapes and spatial distributions. A distinction commonly done in the literature is between spherical pores and non-spherical pores (Sharratt, 2015). The voids observed between the layers are referred to as "acicular pores" by some authors (Smith *et al*., 2016) and they are characterized by an elongated shape. Fig. 2 shows an example of two internal pores of spherical shape, Fig. 2 a), and one acicular pore or irregular and elongated shape, Fig. 2 b), from the study of Tammas-Williams *et al*., 2015. The former have a diameter of few microns, whereas the latter is more than 20 µm in length. The same authors also showed that the pores may be either spread inside the bulk or located mainly between the internal hatching area and the external border (a.k.a. under-skin pores). Pores may be found on the external surface as well. In this case, they are usually referred to as "surface porosity".

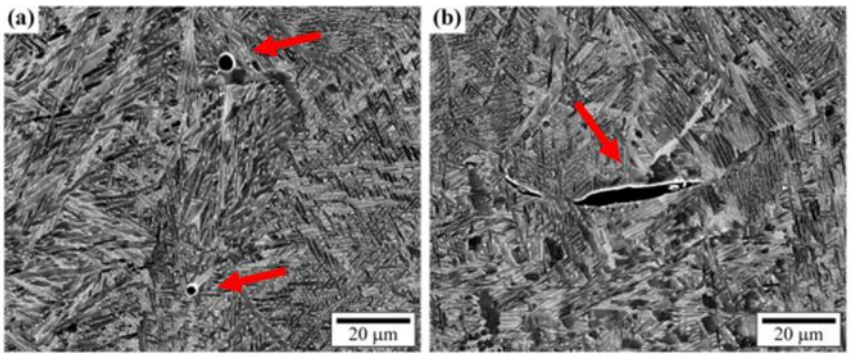

Fig. 2 – Example of two internal spherical pores (a) and one acicular pore (b) in EBM from Tammas-Williams *et al*., 2015 (SEM images).

2.2.2. Residual stresses, cracking and delamination

Residual stresses in SLM have been pointed out to arise from two different mechanisms (Mercelis and Kruth, 2006), including the thermal gradient mechanism and the cool-down phase of molten top layers. As a consequence of a stress relief through fracturing when the tensile stress exceeds the ultimate tensile strength of the solid material at a given point and temperature, **cracking** phenomena occur (Harrison *et al.,* 2015; Carter *et al*., 2014). The different material-dependent mechanisms for which cracks may originate in PBF were studied by different authors (Carter et al., 2014; Harrison *et al.,* 2015; Zhong *et al*., 2005; Dye *et al*., 2001). **Delamination** is a particular case of cracking, where cracks originate and propagate between adjacent layers (inter-layer cracking). When the residual stresses exceed the binding ability between the top layer and the previous one, delamination occurs (Zah and Lutzmann, 2010). A particular case of delamination has been reported by different authors (Mercelis and Kruth, 2006; Zaeh and Branner, 2010) regarding the partial disconnection of the part from the baseplate. Fig. 3 shows an example of macroscopic cracking and delamination in SLM of M2 HSS parts.

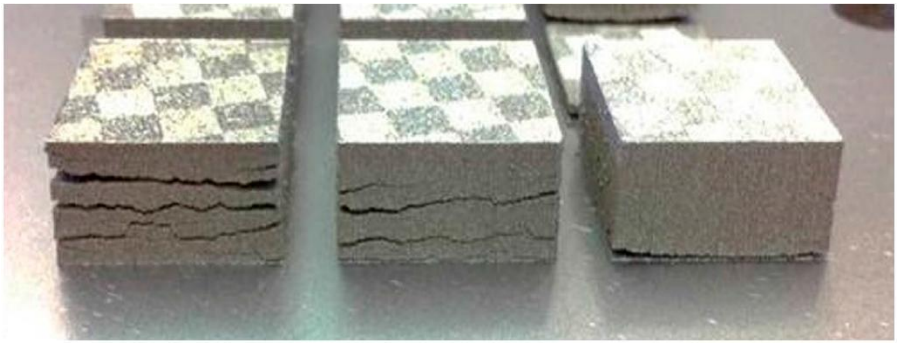

Fig. 3 – Example of severe delamination and cracking in SLM of M2 HSS parts (Sames *et al*., 2016)

2.2.3. Balling

Melt ball formation, a.k.a. balling, occurs when the molten material solidifies into spheres instead of solid layers, which is a severe impediment to interlayer connection (Kruth *et al*., 2004). Surface tension drives the balling phenomenon, by preventing the molten material to wet the underlying layer. The result is a rough and bead-shaped surface that produces an irregular layer deposition, with detrimental effects on the density and quality of the part. Li *et al*., 2012 discussed three disadvantageous effects of the balling phenomenon in SLM. First, it can increase the surface roughness. Second, a large number of pores can be formed between the discontinuous metallic balls. Third, in case of very severe balling, the spheres protruding from the powder layer may interfere with the movement of the powder deposition system. Fig. 4 shows an example of SEM images showing the balling effect on single scan tracks corresponding to different scan speeds (Li *et al*., 2012).

The balling phenomenon as studied by different authors both in SLM (Tolochko *et al*., 2004; Li *et al*., 2012; , Zhou *et al*., 2015; Kruth *et al*., 2007) and EBM (Zah and Lutzmann, 2010).

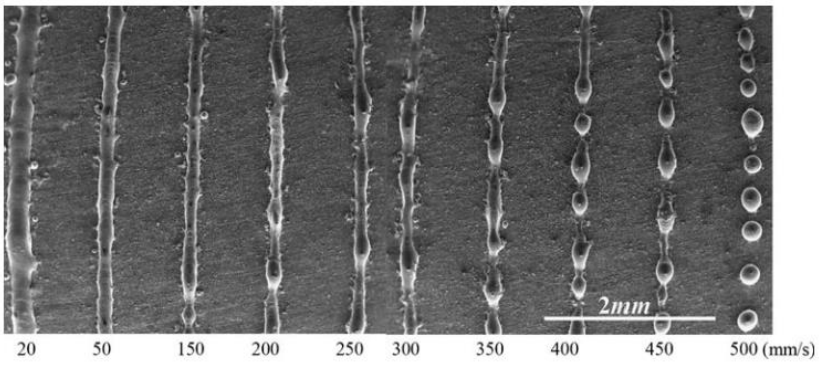

Fig. 4 – Examples of balling effects is SLM on single scan tracks corresponding to different scan speeds, from Li *et al*., 2012 (SEM images)

2.2.4. Geometric defects and dimensional accuracy

The PBF-produced parts may exhibit different kinds of dimensional and geometric deviations from the nominal model. Regarding the size of the part, **shrinkage** has been reported by different authors (Thomas, 2009; Sharratt, 2015), even though the opposite effect (i.e., parts that are systematically larger than the nominal) is not uncommon. In addition to shrinkage and oversizing, warping represents a common source of inaccuracy in PBF. Different kinds of **warpings** were discussed in the literature (Sharratt, 2015). Mousa (2016) investigated the curling phenomenon, i.e., a combination of shrinking and warping that yields a curved profile of down-facing surfaces intended to be flat. Curling is usually associated to an uneven shrinkage between the top and the bottom of the part. Another kind of geometrical distortion observed and investigated by different authors is related to the formation of **super-elevated edges** (Yasa *et al*., 2009; Kleszczynski et al., 2012), i.e., elevated ridges of the solidified material at the edges of the successive layers. This defect strongly impacts the quality and stability of the process for different reasons (Yasa *et al*., 2009). First, it deteriorates the surface topology and the dimensional accuracy of the part. Second, it may worsen the stair-stepping effect due to the layer-wise production. Third, when super-elevated edges protrude from the powder layer, they may interfere with the recoating system, increasing its wear and negatively affecting the consequent powder bed uniformity.

Other distortions affect critical features like thin walls, overhang surfaces and acute corners (zur Jacobsmühlen *et al*., 2013; Grasso *et al*., 2016). In those regions, the melt pool is largely surrounded by loose powder, which has a lower conductivity of the solid material. The diminished heat flux yields local over-heating phenomena that may deteriorate the geometric accuracy. As an example, Fig. 5 shows defects occurred in correspondence of over-hanging acute corners of complicated shapes (a) or wrongly supported parts (b) in SLM (Grasso *et al*., 2016).

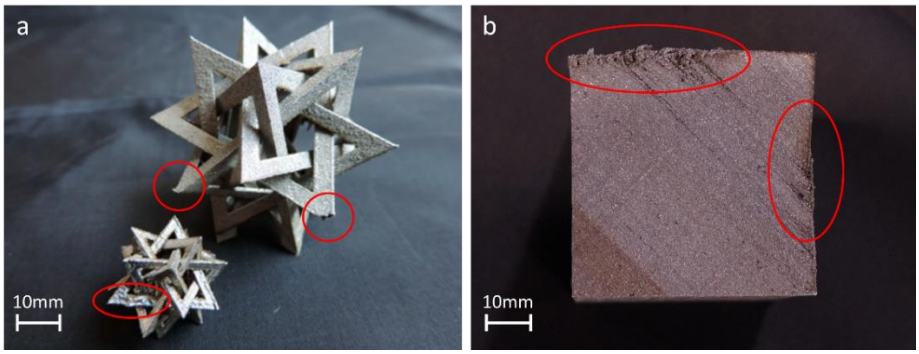

Fig. 5 – Example of geometrical errors in over-hang acute corners (a) or wrongly supported sides (b) in SLM from Grasso *et al*., (2016)

2.2.5. Surface defects

In PBF processes, surface roughness has two contributors, i.e., the stair-stepping effect due to the layer-wise production, and the actual roughness of the metal surface. The surface finishing depends on the surface orientation with respect to the growth direction (Fox *et al*., 2016, Strano *et al*., 2013). In particular, downward- and up-ward surfaces are known to have considerably different roughness properties (Triantaphyllou *et al*., 2015). Although in most cases, PBF-produced parts are post-processed (e.g., surface and thermal treatments), the surface finishing is technologically relevant as it has an effect on the fatigue performances of the part. Because of this, out-of-control roughness and surface characteristics represent one kind of defect in PBF studied by different authors (Sames et al., 2016; Fox *et al*., 2016). Surface defects are also produced by the balling effect, which prevents the achievement of smooth surfaces (Li *et al*., 2012, Strano *et al*., 2013; Townsend *et al*., 2016).

2.2.6. Microstructural inhomogeneities and impurities

PBF processes involve highly localized high-heat inputs during very short beam-material interaction times that will therefore significantly affect the microstructure of the part (Thijs et al., 2010). Microstructural inhomogeneities or non-equilibrium microstructures, together with above mentioned defects, may have a detrimental effect on the mechanical and functional performances of the part. Song *et al*. (2015) reviewed the differences in microstructure between SLM and traditional manufacturing processes, highlighting the relationship between microstructural properties and the formation of micro-pores, cracks and residual stresses. Inhomogeneities of the microstructure include i) impurities, ii) grain size characteristics and iii) crystallographic textures (Sharratt, 2015). Impurities in the material include **inclusions**, **contaminations** from other materials and formations of **surface oxides** (Niu and Chang, 1999; Huang *et al*., 2016). The presence of unfused powders within pores and/or in the form of satellite powder clumps were discussed by some authors (Smith *et al*., 2016, Niu and Chang, 1999). Casati *et al*. (2016) studied the effect of microstructural defects on the fracture behaviour of AISI 316L steel in SLM. Fig. Fig. 6 shows an example of large defects likely originated

from oxides (left panel) and the presence of partially molten particles (right panel) in specimen fracture surfaces (Casati et al., 2016). Both the oxide inclusions and partially molten particles are indicated by arrows in Fig. 6 a) and b), respectively. Such particles are believed to be responsible for the premature failure of the specimens and for the reduced strength because of the effective cross-sectional area reduction.

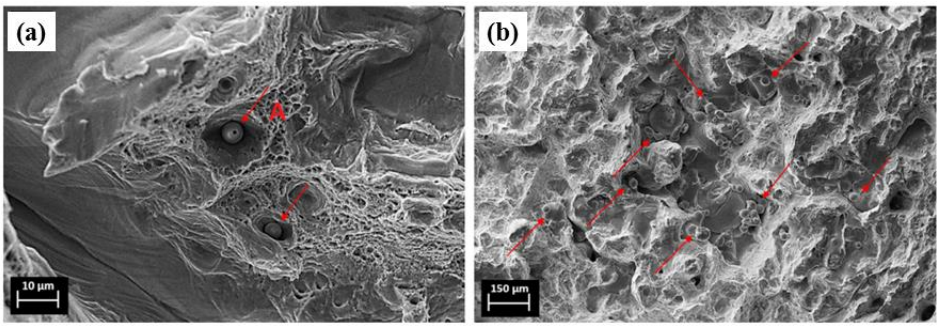

Fig. 6 – (a) examples of two local oxide contaminations indicated by the red arrows in the fracture surface of an AISI 316L specimen in SLM; (b) examples of partially molten particles indicated by the red arrows in the same specimen (re-edited from Casati *et al*., 2016)

2.3. Sources of defects

Accordingly to Sharratt (2015), the defects and errors in metal AM can be grouped into the following categories: 1) **equipment-induced defects**, 2) **process-induced defects** and 3) **model (or design for additive choice)-induced defects**. A forth category can be envisaged, which consists of defects induced by the feedstock material (i.e., the **powder**). The following subsections review the different categories of defect causes, in order to provide a general overview about the origin, evolution and propagation of defects in PBF processes.

2.3.1. Equipment

Equipment-induced defects are caused by improper performance, setting and calibration of the main system components. They can be further classified into the following sub-categories: i) defects induced by the beam scanning/deflection system, ii) defects induced by the build chamber environmental control, iii) defects induced by the powder handling and deposition system, and iv) defects induced by insufficient baseplate thickness. One source of geometric defects and low accuracy is associated with the **beam scanning or deflection system**. Moylan *et al*. (2014b) pointed out the effect of the quality of the optical system alignments, the quality of the mirrors, imperfections of the f-θ lens, and the profile of the laser beam in SLM. A miscalibrated system can result in parts with inaccurate final dimensions (Foster *et al*., 2015). In addition, there is a known exposure location effect on the shape of the beam spot (Foster *et al*., 2015). An elliptical distortion of the laser spot in SLM occurs near the edges of the baseplate due to high scanner deflection angles, which inflate the effect of angular inaccuracies of the galvanometers further from the baseplate center. This kind of error can lead to lack of fusion and produce different defects, including porosity and poor

geometric accuracies depending on the location where the part is built. The contamination from gaseous byproducts or the reflected energy from the powder bed may influence the local beam spatial energy distribution, leading to poor part accuracy as well. Other defects are related to the control of the chamber environment (Van Elsen, 2007; Sames *et al*., 2016). SLM processes operate in an **inert environment**, with argon or nitrogen flowing over the build surface. The flow rate of the fill gas, its pathway and laminarity are known to have a direct impact on various defects, including porosity and geometrical accuracy (Ferrar *et al*., 2012). In laser welding processes, small changes in **oxygen composition** have been observed to yield relevant shape variations of the melt pool affecting the process stability (Lu *et al*., 2004; Zhao *et al*., 2010), and similar effects have been discussed for SLM (Spears and Gold, 2016). The oxygen content in the building chamber was shown to be critical for the balling effect initiation as well (Li *et al*., 2012).

Defects associated to warpings, deformations, layer delaminations and cracks are influenced by the **thickness of the baseplate** and the way the process heat is dissipated through the baseplate (Prabhakar *et al*., 2015). Indeed, the use of an insufficient baseplate thickness can significantly affect the heat dissipation and inflate solidification-related thermal stresses (Zeng, 2015). The **pre-heating** of the powder bed is important to lower thermal gradients and stresses as well. The choice of improper pre-heating settings is a possible cause of residual stress development (Leuders *et al*., 2013; Edwards *et al*., 201; Chlebus et al., 2011; Buchbinder *et al*., 2014). Kempen *et al*. (2013) studied the effects of baseplate pre-heating in SLM, showing that pre-heating is not only a countermeasure against residual stresses and consequent deformations, but it also enables the enhancement of the final part density.

Another equipment that can induce defects is the **powder handling and deposition system**. In most cases (Kleszczynski *et al*., 2012; Foster *et al*., 2015), the wear of the recoating system and the deposition of a inhomogeneous powder bed is not the root cause of observed defects, but a consequence of powder bed contaminations (see below a discussion on defects induced by spatters) or super-elevated edges that protrude from the thin powder layer (Kleszczynski *et al*., 2012). However, because of the linear motion of the recoating system, defects originated in some area of the layer may propagate along the recoating direction. Uneven powder layers have a detrimental effect on the physical interaction between the laser beam and the material resulting in inconsistent processing and, in some cases, porosity (Foster *et al*., 2015).

2.3.2. Process

Process-induced defects are associated with the interaction between the beam, the loose powder, and the previously melted material. The effect of **process parameters** and **scan strategies** on the onset of different kinds of defects has been studied by many authors in the recent years for different materials both in SLM and EBM (see Table 1). The scan strategy influences the temperature distribution over the slice (Van Elsen, 2007). Therefore, wrong strategies, depending on the part geometry, may increase the residual stresses (Mercelis and Kruth, 2006; Parry *et al*., 2016; Cheng *et al*., 2016). Previous studies (Van Belle *et al*., 2013;

Casavola *et al*., 2008) showed that the layer thickness influences the residual stresses in the part and the balling phenomenon initiation (Li *et al*., 2012) as well. In addition, improper strategies may inflate the generation of super-elevated edges (Yasa *et al*., 2009) and affect the microstructural properties of the part (Carter *et al*., 2012; Arisoy *et al*., 2016). Matthews *et al*., (2016) and Yasa *et al*. (2009) discussed the scan strategy effect on porosity and void generation. In particular, improper hatch spacing may produce linear void structures associated with the powder denudation effect, i.e., the apparent clearing of powder around a single track bead (Matthews *et al*., 2016). The effects of various process parameters on part density for many materials have been investigated by different authors (see Table 1). The laser power, the scan speed and the hatch distance determine the **energy density** (i.e., energy per surface unit) transferred to the material and hence most of the studies in the literature focused on these parameters. These studies demonstrated a correlation between the energy density and the part density and allowed identifying a window of process parameters corresponding to good part density and quality. The study of Gong (2013) outlined different regions in the parameter space spanned by laser power and scan speed in SLM of Ti6Al4V (Fig. 7): zone I corresponds to fully dense parts, zone II to over-melting conditions, zone III to incomplete melting and zone OH to over heating parameters.

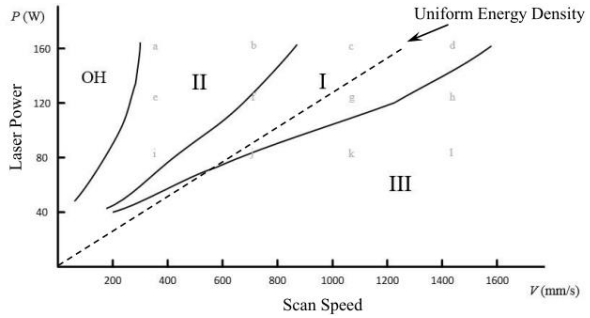

Fig. 7 – Good quality process window (I) and defecting zones (II, III, OH) with respect to scan speed and laser power in SLM of Ti6Al4V (Gong, 2013)

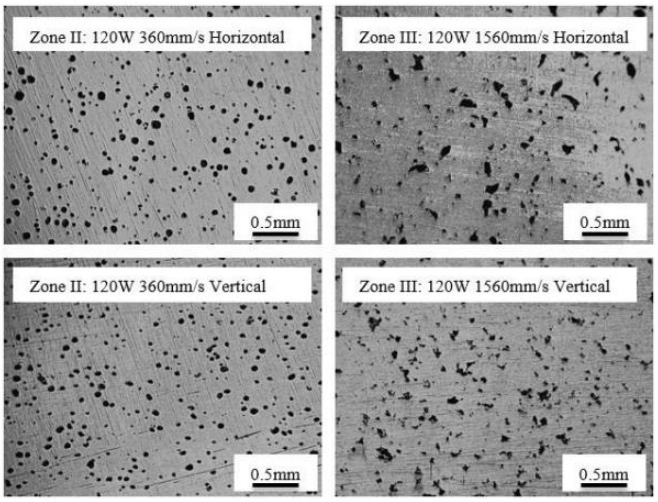

Fig. 8 – Porosity in horizontal (top panels) and vertical (bottom panels) cross-sections of SLM-produced Ti6AL4V specimens under over-melting (zone II) and insufficient melting (zone III) conditions (Gong, 2013)

Gong (2013) showed that zone II (over-melting, high energy density) and zone III (incomplete melting, low energy density) also correspond to different morphological characteristics of the internal porosity (Fig. 8).

The energy density plays an important role to determine the balling phenomenon, too. Li *et al*. (2012) showed that increasing the energy density (high power and low scan speed) allows mitigating or avoiding this kind of defect. Regarding EBM, different authors (Scharowsky *et al*. (2015), Zaeh and Kahnert (2009), Puebla *et al*. (2012), Tammas-Williams *et al*. (2015) and Biamino *et al*. (2011) studied the importance of process parameters and scanning strategy of part density, pore morphology and part performances.

Another source of defects is related to the **particle and liquid metal ejections** due to the interaction between the beam and the material. Such ejections are mainly caused by i) a convective transport of liquid or vapourised metal out of the melt pool, ii) non-molten metallic powder particles blown away as a result of the impact of metallic vapor, iii) the electrostatic repulsion of powder particles in EBM (Sames *et al*., 2016; Liu *et al*., 2011). The first two types of ejections are referred to as “droplet spatters” and “powder (or sideways) spatters”, respectively (Liu *et al*., 2011). The spatter generation mechanism was studied in depth by Khairallah *et al*. (2016) and Liu *et al*. (2015). When the spatters fall on the powder bed, they can produce two kinds of defects. When the beam passes over the deposited spatter, its larger size may prevent complete melting, which can result in formation of voids within the part. On the other hand, if the spatter is displaced by the recoating device (particle dragging), an irregularity of the powder bed can be produced, leading to a discontinuity in the material (Gong, 2013). The control of the shape of the laser power profile in SLM, or pulse shaping, was pointed out as a method to increase energy absorption and decrease spatter ejections (Mumtaz and Hopkinson, 2010). In the EBM process, an additional particle ejection phenomenon is related to electrostatic forces. Indeed, electrons interact with the material transmitting both energy and electrical charge. When repulsive electrostatic forces overwhelm the forces holding particles to the powder bed, powder particles ejection may occur (Mahale, 2009; Eschey *et al*., 2009). Besides spatters, in some particular cases, the formation of plasma due to the ionization of the metallic vapor and the surrounding gas has been reported (King *et al*., 2014). The vapor formation and the heating of the surrounding gas result in the formation of the plume, which differs from the surrounding atmosphere in terms of chemical composition, temperature and pressure. It can induce changes in the optical properties of the beam path, which may alter the beam profile and energy density on the material surface (Wang *et al*., 2011). In SLM a plasma/metal vapour plume can change the absorptivity along the pool depth (Khairallah *et al*., 2016)

2.3.3. Build preparation choices

Model-induced errors mainly arise from the choices implemented during the AM build design stage, with particular reference to i) the design of supports and sacrificial components and ii) the orientation of the part with respect to the baseplate and the SLM/EBM reference system. **Supports** are needed i) to guarantee proper mechanical sustain for down-facing (overhang) regions (i.e., avoid collapses when new layers are

deposited), ii) to provide the correct heat exchange towards the building platform, and iii) to keep the part from excessive warping caused by high residual stresses (Gibson *et al*., 2010). The selection and design of supports is one of most important steps of the build design stage, which has a strong impact on the final part quality and performances (Foster *et al*., 2015; Kleszczynski *et al*., 2012; Zeng, 2015; Grasso *et al*., 2016). The **part orientation** on the baseplate has a direct effect on product quality and performances too. Delgado *et al*. (2012) studied the effect of the build direction on the part quality in SLM, and they highlighted the influence in terms of dimensional accuracy and surface roughness. Moreover, the anisotropic behaviour of the final product is strongly related to the build direction of the part, which eventually influences its mechanical and physical properties (Meier and Haberland, 2008).

2.3.4. Powder

The quality of the feedstock material is of great importance for the quality and performances of the final part. In PBF, the quality of powders is directly related to the production process (e.g., gas atomization, water atomization, plasma atomisation, etc.). **Flowability** and **apparent density** have been pointed out to have a major impact on product qualities (Sames *et al*., 2016). Spherical and smooth particles improve both these two properties, whereas the use of fine particles may improve the apparent density but it may reduce the flowability, with detrimental effects on the final density of the part (Liu *et al*., 2015; Van Elsen, 2007). A typical particle size range of powders used in SLM is 10 – 45 µm and in EBM is 45 – 106 µm (Advanced Powders, 2016). Slightly thicker layers and powder sizes are used in EBM. Indeed, it was shown that reducing the average particle size yields no noticeable effect on chemistry, mechanical and microstructural properties of EBM produced parts (Karlsson *et al*., 2013). Metallic powders may be contaminated by moisture, organics, adsorbed gases, oxide and nitride films on particle surfaces (Das, 2003). Such a **contamination** may degrade the mechanical properties and the geometrical accuracy of the consolidated component in SLM (Das, 2003). Tang *et al*. (2015), Seyda *et al*. (2012), Hann (2016) and Ardila *et al*. (2014) studied the powder property changes after several re-use cycles.

3. IN-SITU SENSING

The NIST report authored by Mani *et al*. (2015) referred to the quantities that can be determined during the AM process as “process signatures”. Accordingly to Mani *et al*. (2015), the process signatures are “dynamic characteristics of the powder heating, melting, and solidification processes as they occur during the build”. Mani *et al*. (2015) also suggested a categorization of these signatures into two classes: i) observable signatures and ii) derived signatures. The former can be observed and measured during the process by using in-situ sensing devices. The latter can be determined through analytical models or simulation. This review is focused on observable signatures and the corresponding in-situ sensing and monitoring approaches.

Subsection 3.1 briefly reviews the different categories of observable signatures in PBF processes, whereas subsection 3.2 reviews the in-situ sensing approaches used and developed by different authors.

3.1. Process signatures

The process signatures can be grouped into four major categories, depending on the level of detail required for process observation. These categories are: i) the melt pool, ii) the track along the scan path, iii) the slice and iv) the powder bed. The term "slice" refers to the slice of the part scanned by the power source in each layer. The term "powder bed", instead, refers to the thin layer of loose powder deposited by the recoating system, before starting the SLM or EBM process of the current layer.

During laser or electron beam irradiation on the metal powders, the **melt pool** is formed, which then solidifies to the consolidated structure. The melt pool is known to be a primary feature of interest in any process that involves a beam-material interaction aimed at achieving a local fusion of the material (Craeghs *et al*., 2010 - 212; Clijsters *et al*., 2014; Berumen *et al*., 2010; Lott *et al*., 2011; Doubenskaia *et al*., 2012 - 2015). Indeed, the stability, dimensions and behaviour of the melt pool determine to a great extent the quality and stability of the process (Thijs *et al*., 2010). In the literature, four main melt pool-related quantities were considered for monitoring purposes: i) the size (i.e., the area or the diameter), ii) the shape, iii) the temperature intensity (average or cumulative), and iv) the temperature profile (1D profiles along the transversal and longitudinal direction or 2D profile over the entire area). The size, shape and temperature of the melt pool are strongly affected by the process parameters, the scanning strategy, and the beam-material interaction, which influence the occurrence of most of defects mentioned in Section 2.2. The melt pool properties determine the geometrical accuracy of the track and surface and geometrical properties of the final part. They also influence the porosity of the part, the partial melting of powder particles and the presence of unmelted particles within the bulk material, together with the development of the residual stresses, cracking and delaminations (Mercelis and Kruth, 2006; Zah and Lutzmann, 2010). The melt pool represents the highest level of detail of in-situ monitoring methods, which imposes different challenges for the measurement viewpoint. First, the in-situ sensing system must be able to measure the characteristics of a very small region (a few hundreds of microns of diameter) with a sufficient spatial resolution. Moreover, a very high sampling rate is needed, since the scanning speed in SLM is in the order of thousands of millimetres per second and it is even higher in EBM.

The final quality and functional performances of the part depend not only on the properties of the melt pool, but also on the properties of each **single track**. In particular, three quantities were considered by different authors (Kanko *et al*., 2016; Krauss *et al*., 2012 – 2014; Bayle and Doubenskaia, 2008; Lane *et al*., 2015; Price *et al*., 2012; Grasso *et al*., 2016): i) the geometry of the track, ii) the temperature profile over the track and iii) material ejected from the melt pool and the surrounding area during the process. The geometry and the temperature profile of the track provide relevant information for the determination of balling phenomena,

lack-of-fusion or local over-heating conditions, surface and geometric errors and porosity formation. In addition, the observation of material ejection is relevant to characterize process byproducts that may affect the quality of the part (Bayle and Doubenskaia, 2008; Lane *et al*., 2015). Analogously to the monitoring of the melt pool, the monitoring of the process along the scan path imposes challenges in terms of required spatial and temporal resolution of the in-situ sensing system.

By further expanding the region of interest, it is possible to gather in-situ data at **slice** level after exposure to the heat source and subsequent solidification. In this case, the main quantities of interest are: i) the surface pattern of the slice, ii) the geometry of the slice (and its departure from the nominal shape), iii) the local thickness profile and iv) the temperature profile over the entire slice area (typically a 2D profile). The analysis of the surface pattern reveals irregularities that may be caused by different defects, including balling, porosity and other kinds of distortions (Kleszczynski *et al*., 2012 – 2014; zur Jacobsmühlen *et al*., 2013). The measurement of the slice geometry allows implementing an in-situ "metrological" system able to reconstruct the actual shape of the printed slice on a layer-by-layer basis (Foster *et al*., 2015). The determination of the slice characteristics allows detecting super-elevated edges and other surface irregularities that may have a strong impact on the wear of the recoating system and the consequent defect propagation within the building area (Kleszczynski *et al*., 2012 – 2014; zur Jacobsmühlen *et al*., 2013). The 2D temperature profile over the slice is another relevant feature to determine irregularities caused by lack-of-fusion or local over-heating (Krauss *et al*., 2014; Mireles *et al*., 2015; Moylan *et al*., 2014a; Rodriguez *et al*., 2012 - 2015).

The last category of observable signatures consists of the **powder bed**. In this case, the signal acquisition can be performed after (or during) the deposition of the powder bed itself, before the SLM/EBM of the next layer is started. The main quantities of interest are: i) the bed uniformity, ii) the temperature and iii) the 2D temperature profile. The in-situ determination of the powder bed uniformity is important to detect rippling caused by recoater bouncing effects and/or rectilinear grooves generated either by particles dragging or other recoating system damages (Foster *et al*., 2015). The temperature stability from one layer to another and the 2D temperature profile in each layer are additional features to be used to characterize the temporal and spatial evolution of the process (Islam *et al*., 2013).

Few studies considered quantities that can not be included into the aforementioned categories, which include the **vibration** of the recoating system (Kleszczynski *et al*., 2014), the **ultrasounds emissions** of the process (Rieder *et al*., 2014), and the part and **baseplate distortion** (Dunbar, 2016). The literature devoted to in-situ sensing and monitoring of PBF processes is summarized in Table 2 with respect to the monitored signatures and the type of process, i.e., SLM or EBM.

Table 2 – Mapping of the literature on in-situ sensing of SLM and EBM with respect to the monitored signatures

Process signatures		Literature on In-situ Monitoring	
		SLM	EBM
Melt pool	**Size**	Craeghs et al., 2010 - 2012; Clijsters et al., 2014; Berumen et al., 2010; Lott et al., 2011; Kruth et al. 2007; Van Gestel, 2015	
	Shape	Craeghs et al. 2011; Berumen et al., 2010; Yadroitsev et al., 2014; Van Gestel, 2015; Kruth et al., 2007; Doubenskaia et al., 2015	
	Temperature intensity	Doubenskaia et al., 2012; Craeghs et al., 2011; Clijsters et al., 2014; Chivel, 2013; Berumen et al., 2010; Pavlov et al., 2010; Yadroitsev et al., 2014; Van Gestel, 2015	
	Temperature profile	Doubenskaia et al., 2012	Gong et al., 2013b; Price et al., 2012
Track (scan path)	**Track geometry**	Kanko et al., 2016; Doubenskaia et al., 2015	
	Temperature / intensity profile	Krauss et al., 2012 - 2014; Lane et al., 2015; Bayle and Doubenskaia, 2008; Schilp et al., 2014; Grasso et al., 2016	Gong et al., 2013b; Price et al., 2012
	Ejected material	Lane et al., 2015; Bayle and Doubenskaia, 2008	
Slice	**Surface pattern**	zur Jacobsmühlen et al., 2013; Kleszczynski et al., 2012; Zhang et al., 2016; Foster et al., 2015; Neef et al., 2014; Erler et al., 2014 (SLS)	Schwerdtfeger et al., 2012; Ridwan et al., 2014
	Geometry	Foster et al., 2015	Ridwan et al., 2014
	Thickness profile	zur Jacobsmühlen et al., 2013 - 2015; Land et al., 2015; Kleszczynski et al., 2012; Zhang et al., 2016	
	Temperature/ intensity profile	Schilp et al., 2014; Wegner and Witt, 2011 (SLS); Krauss et al., 2014; Grasso et al., 2016	Rodriguez et al., 2012 - 2015; Dinwiddie et al., 2013; Price et al., 2014
Powder bed	**Homogeneity**	Foster et al., 2015; Neef et al., 2014; Erler et al. 2014 (SLS)	
	Temperature intensity	Islam et al., 2013; Dunbar, 2016	
	Temperature profile	Wegner and Witt, 2011 (SLS)	
Other	**Recoating system vibration**	Kleszczynski et al., 2014; Reinarz and Witt, 2012, zur Jacobsmühlen et al., 2015	
	Ultrasound emission	Rieder et al., 2014	
	Part distortion	Dunbar, 2016	

Table 2 shows that the number of studies in SLM is greater than the one in EBM. One possible explanation for this is related to the current existence of different SLM system producers (EOS, Concept Laser, Renishaw, SLM Solutions, Phenix and others), but only one EBM system producer (Arcam). Second, in SLM systems it is possible to exploit the laser optical path to monitor the melt pool. This is not possible in EBM because the electron magnetic coils that deflect the electron beam prevents from a co-axial sensor integration. In addition, the scanning speed in EBM is higher than in SLM, which makes the continuous monitoring of the melt pool and the heat affected zone during the process more challenging.

Table 3 – Mapping of the literature on in-situ sensing of SLM and EBM with respect to the monitored signatures and the sensing approach (italic font used for co-axial set-ups and roman font for off-axial set-ups)

Monitored signature		In-situ sensing (main categories)			
		Pyrometry	**Imaging (visible to NIR)**	**Thermal imaging (NIR to LWIR)**	**Interferometric imaging**
Melt pool	**Size**	*Clijsters et al., 2014; Craeghs et al., 2010 - 2011;*	*Craeghs et al., 2010 - 2012; Clijsters et al., 2014; Berumen et al., 2010; Kruth et al., 2007; Van Gestel, 2015*		
	Shape		*Craeghs et al., 2011; Berumen et al., 2010; Van Gestel, 2015; Kruth et al., 2007*	Doubenskaia et al., 2015	
	Temperature intensity	*Craeghs et al., 2011; Berumen et al., 2010; Chivel, 2013; Clijsters et al., 2014; Doubenskaia et al., 2012; Pavlov et al., 2010; Thombansen et al., 2015;*	*Berumen et al., 2010; Van Gestel, 2015; Yadroitsev et al., 2014; Chivel, 2013;*		
	Temperature profile		*Doubenskaia et al., 2012;*	Gong et al., 2013b; Price et al., 2012	
Track (scan path)	**Track geometry**			Doubenskaia et al., 2015	*Kanko et al., 2016*
	Temperature/ intensity profile	Bayle and Doubenskaia, 2008; *Thombansen et al., 2015*	Grasso et al., 2016	Krauss et al., 2012 - 2014; Lane et al., 2015; Bayle and Doubenskaia, 2008; Gong et al., 2013b; Price et al., 2012; Schilp et al., 2014;	
	Ejected material	Bayle and Doubenskaia, 2008		Bayle and Doubenskaia, 2008; Lane et al., 2015	
Slice	**Surface pattern**		Foster et al., 2015; zur Jacobsmühlen et al., 2013; Kleszczynski et al., 2012; Zhang et al., 2016	Ridwan et al., 2014; Schwerdtfeger et al., 2012; Mireles et al., 2015; Dinwiddie et al., 2013	*Neef et al., 2014*
	Geometry		Foster et al., 2015	Ridwan et al., 2014	
	Thickness profile		zur Jacobsmühlen et al., 2013 - 2015; Kleszczynski et al., 2012; Land et al., 2015; Zhang et al., 2016		
	Temperature/ intensity profile		Grasso et al., 2016	Krauss et al. 2014; Rodriguez et al., 2012 - 2015; Schilp et al., 2014; Wegner and Witt, 2011; Dinwiddie et al., 2013	
Powder bed	**Homogeneity**		Foster et al. 2015;		*Neef et al., 2014*
	Temperature intensity	Islam et al., 2013			
	Temperature profile			Wegner and Witt, 2011	

3.2. In-situ sensing equipment and set-ups

The mainstream sensors and in-situ data collection devices proposed in the literature can be grouped into the following major categories: i) non-contact temperature measurements (i.e., pyrometers and infrared (IR) imaging), ii) imaging in the visible range, iii) low-coherence interferometric imaging. A further important categorization regards the sensor mounting strategy, which involves either "co-axial" or "off-axial" systems. In co-axial configurations, the sensors exploit the optical path of the power source. As mentioned above, this only applies to SLM. In off-axial configurations, the sensors are placed outside the optical path, with a given angle-of-view with respect to the region of interest. Table 3 maps the literature with respect to these proposed sensing systems and the corresponding monitored signatures. Imaging systems are divided on the basis of the monitored spectrum, i.e., from visible to Near Infrared (NIR) and from NIR to Long wavelength Infrared (LWIR). Italic fonts were used to denote the references where a co-axial mounting was proposed, whereas roman fonts are used to denote references where an off-axial was applied instead. The mainstream sensing methods summarized in Table 3 are reviewed in subsection 3.2.1 and 3.2.2.

In addition to the above categories, other proposed sensors include: i) 2D laser displacement sensors, ii) optical coherence tomography devices, iii) accelerometers, iv) ultrasound detectors, v) strain-gauges, vi) thermo-couples and vii) X-ray detectors. A review of the literature devoted to these systems is discussed in subsection 3.2.3.

3.2.1. Co-axial sensing

Different authors developed a co-axial setup to monitor melt pool-related quantities in SLM. A research group from the Katholieke Universiteit Leuven developed a patented co-axial monitoring system that is exclusively licensed by Concept Laser (Berumen *et al*., 2010, Clijsters *et al*., 2014; Craeghs *et al*., 2010 - 2012; Kruth *et al*., 2007). The system is shown in Fig. 9. The optical set-up includes a high-speed NIR CMOS camera and a photodiode (whereas in Craeghs *et al*., 2010 the CMOS camera was not a thermal one). The laser beam (1064 nm) is reflected by a partially reflective mirror towards the scanner, and the same mirror enables the radiation emitted by the melt pool (780 – 950 nm) to be captured by the two sensors. The partially reflective mirror reflects the light at the laser wavelength of 1064 nm towards the laser source, whereas the radiation at other wavelengths pass through the mirror. This radiation is then split towards the two sensors, which are both sensitive to wavelengths in the range of 400 – 1000 nm. The incoming radiation is integrated into one value representing the melt pool intensity. The NIR camera is equipped with a 1280 x 1024 pixel CMOS sensor that enables determination of the geometry and temperature distribution of the melt pool as well. This camera is used to determine the shape and size of the melt pool. The sample rate for both the sensors is 10 kHz, which means that two consecutive data samples are spaced apart of 100 µm along the scanning path at a speed of 1000 mm/s. However, the 10 kHz sampling rate can be achieved by the NIR camera only by reducing the field-of-view to a limited region of interest (Berumen *et al*., 2010).

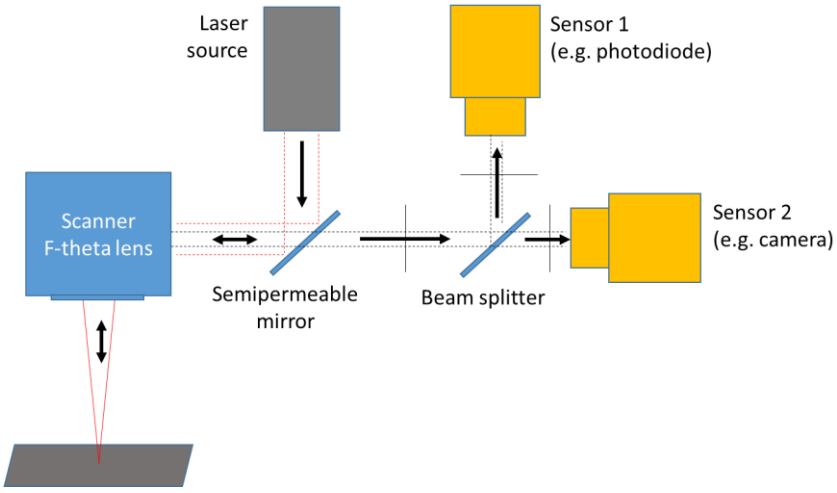

Fig. 9 – Co-axial sensing set-up for SLM process monitoring (scheme re-edited from Craeghs *et al*., 2010)

Another co-axial monitoring set-up was presented by Doubenskaia *et al*. (2012), Chivel (2013), Pavlov *et al*. (2010) and Yadroitsev *et al*., 2014. In this case, the melt pool temperature intensity is captured by a two-wavelength pyrometer connected to the optical unit by an optical fiber. The pyrometer includes two InGaAs photodiodes with a temperature range of 1200-2900 K, a transmission spectrum at central wavelength 1260 nm with a 100 nm bandwidth, and a measured area with a diameter of 560 µm (a 1.4 magnification was used). A CCD camera with a resolution of 560 x 760 pixels was used to measure the image brightness profiles along the transversal and longitudinal directions. The sampling frequency used by Doubenskaia *et al*. (2012), Chivel (2013) and Pavlov *et al*. (2010) is 20 kHz, with a scanning velocity of 120 mm/s. More recently, a co-axial set-up was proposed by Van Gestel (2015), where one or two CMOS cameras (with wavelength sensitivity between 400 and 1000 nm) were used to determine the melt pool size, shape and intensity.

Lott *et al*. (2011) and Thombansen et al. (2015) proposed another version of the co-axial monitoring set-up for SLM with two major differences: the presence of a co-axial laser illumination source (Lott *et al*., 2011; Thombansen *et al*., 2015) and a pre-focusing unit (Thombansen *et al*., 2015). The pre-focusing unit is used to avoid axial and lateral chromatic aberrations due to the different imaging properties of f-θ lens at wavelengths different from the processing one. In particular, it ensures that the focal plane is the same at every wavelength of interest. The illumination beam is deflected by a beam splitter and transmitted to the dichroic mirror. The radiation emitted by the melt pool is transmitted through the dichroic mirror and the beam splitter towards a high-speed camera and a pyrometer. The illumination systems enhances the visualization of the melt pool dynamics.

A different co-axial sensing technique was proposed by Kanko *et al*. (2016) and Neef *et al*. (2014). It consists of a low-coherence interferometric technique, also termed inline coherent imaging (ICI), suitable for co-axial monitoring of the SLM process at high frequency. A typical ICI system consists of low-power broadband light source (e.g., a super-luminescent diode (SLD)), a high-speed spectrometer and a fiber-based Michelson

interferometer (Kanko *et al*., 2016). Neef *et al*. (2014) first proposed this approach for powder bed uniformity analysis and monitoring of the surface slice patterns. The proposed set-up is based on the PRECITED IDM sensor, with a maximum scan rate of 70 kHz. Neef *et al*. (2014) discussed different possible applications and showed an example of surface topology reconstruction for both loose powder and molten material. Kanko *et al*. (2016) extended the same technique to the monitoring of the melt pool morphology, with a frame rate of 200 kHz. Kanko *et al*. (2016) showed that the ICI technique is suitable to measure the intensity, height and longitudinal dimension of the melt pool along single tracks, which allows detecting different kinds of defects, including balling, lack-of-fusion, over melting and other surface irregularities.

3.2.2. Off-axial sensing

In SLM, different authors proposed the use of off-axial cameras for in-situ monitoring, either in the IR or visible range. These cameras can be used to gather information i) during the scanning of each track/slice, ii) at the end of the SLM of one complete layer or iii) before starting the SLM of a new layer, after the powder bed has been deposited. In the first case, high-speed vision systems are needed, whereas in the latter two cases low-speed but high spatial resolution cameras are used.

Table 4 summarizes the main set-up parameters proposed by different authors in SLM.

In the studies of Krauss *et al*. (2012), Moylan *et al*. (2014a), Wegner and Witt (2011), Lane *et al*. (2015), Bayle and Doubenskaia (2008), Doubenskaia *et al*. (2015) and Schilp *et al*. (2014) a **thermal camera** was used. Differently from the studies discussed in subsection 3.2.1, IR cameras used by these authors in off-axial configurations have detectors with sensitivity that ranges from short to long-wavelength IR. The cameras were mounted outside the building chamber, which imposed the use of a germanium or B270 superwhite glass shield (Krauss *et al*., 2012; Lane *et al*., 2015). This kind of set-up was used to acquire the thermogram of the heat affected zone and surrounding areas along the scan path. The acquired thermal videos were also suitable to observe the spatter ejection produced by the beam-material interaction.

Bayle and Doubenskaia (2008) proposed coupling the off-axis IR camera with an off-axis pyrometer in order to monitor the temperature evolution during the SLM of each slice and to observe the spatters ejected by the beam-material interaction. The pyrometer includes an InGaAs detector with wavelength range of 1001 – 1573 nm, spatial resolution of 800 µm and sampling frequency of 20 kHz. An off-axis pyrometer for powder bed monitoring was used by Islam *et al*. (2013), too.

Table 4 – Main set-up parameters and setting proposed by authors for off-axial monitoring of SLM processes

Reference	Camera type	Wavelength range	Field of view	Lens and filters	Frame rate	Spatial resolution
Krauss et al., 2012, Schilp et al., 2014	Infratec Variocam hr head	8000 – 14000 nm	160x120 mm	50 mm telephoto lens	50 Hz	250 µm/pixel
Lane et al., 2015	extended sensitivity range InSb camera	<1000 nm to 5300 nm	12.96x6.82 mm	50 mm shirt-wavelength IR lens and filters	1800 Hz	36 µm/pixel (horizontally) 53.3 µm/pixel (vertically)
Bayle and Doubenskaia, 2008, Doubenskaia et al., 2015	FLIR Phoenix RDAS with InSb sensor	3000 – 5000 nm	6.4x13.6 mm in sample images	25 mm lens	From 2031 to 3556 Hz	100 µm/pixel
Wegner and Witt, 2011	InfraTec Jade III MWIR camera	3000 – 5000 nm	Entire build area (setup A), 2/3 build area (setup B)	50 mm telephoto lens	700 Hz	1.5mm/pixel (setup A) 350 µm/pixel (setup B)
Kleszczynski et al., 2012 Jacobsmulhen et al., 2013 – 2015	Monochrome SVCam-hr29050, SVS-VISTEK GmbH	visible	130x114 mm	Hartblei Macro 4/120 TS Superrotator	Not relevant to the application	24 µm/pixel
Land et al., 2015	Single-lens reflex camera + fringe projector	visible	Entire build area	Unknown	Not relevant to the application	Unspecified
Zhang et al., 2016	PointGray Flea3 camera + fringe projection	visible	28x15 mm	50 mm lens	Not relevant to the application	6.8 µm/pixel
Foster et al., 2015	Nikon D800E	visible	250x250 mm (lens A), 135x62/78 mm (lens B)	28 mm f/2.8 (lens A), 105 mm f/2.8 (lens B)	Not relevant to the application	50 µm/pixel (lens A), 15 µm/pixel (lens B)
Grasso et al., 2016	Olympus I-speed 3 camera	visible	60x60 mm	SIGMA 105 mm macro lens	300 Hz	About 150 µm/pixel

In the studies of Land *et al*. (2015), Kleszczynski *et al*. (2012), zur Jacobsmühlen *et al*. (2013 – 2015), Foster *et al*. (2015) and Grasso *et al*. (2016) a camera in the **visible range** was used. Kleszczynski *et al*. (2012 and, Jacobsmulhen *et al*. (2013 – 2015) used a monochrome CCD camera (36 by 24 mm Kodak 29 mepapixel sensor) mounted outside the build chamber. The spatial resolution was 24 µm/pixel for a field of view of about 130x114 mm. Two images per layer were acquired, one after the powder deposition and one after the SLM of the layer. Thus, the frame rate is not a relevant parameter in this case. An illumination system was used, including matte reflectors for diffuse lighting on the back of the machine and powder blade, illuminated by two directed sources from the front and right, respectively. This set-up was used by Kleszczynski *et al*. (2012) and zur Jacobsmühlen *et al*. (2013 – 2015) to monitor the surface pattern of the scanned slices and the homogeneity of the powder bed. Foster *et al*. (2015) used a 36.3 megapixel single lens reflex (SLR) camera mounted inside the build chamber with multiple flash modules to collect multiple pictures with varying illumination both after powder bed deposition and again after SLM. The lens used for the analysis presented by Foster *et al*. (2015), 28 mm lens, allowed achieving a resolution of about 50 µm/pixel across the entire 250 x 250 mm baseplate. Land *et al.* (2015) proposed a monitoring system that involves an off-axis SLR

camera in the visible range and a fringe projector. Fringe projection was proposed also by Zhang and Attar (2015). Once the system has been calibrated, the fringes can be projected, shifted and captured by the camera. The result is a topography map (3D point cloud corresponding to a field of view of 28x15 mm with 6.8 µm/pixel resolution) of both the scanned slice and the un-melted powder surface. Land *et al.* (2015) and Zhang *et al*. (2016) showed that this measurement system is suitable to measure the height profile of each layer. Zhang *et al*. (2016) showed that surface patterns of the scanned slice can be captured as well. Therefore, this system can be used for the detection of defects related to local elevated edges and surface irregularities, but it is suitable for geometric slice reconstruction as well. For a similar purpose, Erler *et al*. (2014) proposed the use of a 2D laser displacement sensor for a 3D powder bed topography reconstruction, aimed at detecting both powder bed inhomogeneities and scanned surface irregularities. The sensor operates accordingly to the principle of optical triangulation, with a spot diameter of 40 x 25 µm. Erler *et al*. (2014) proposed a linear axis system to move the sensor over the powder bed surface.

All the above mentioned set-ups (apart from the one discussed by Erler *et al*., 2014) in the visible range were aimed at acquiring single images of the powder bed and the scanned slices. On the contrary, Grasso *et al*. (2016) presented a study to monitor the SLM process by using a high-speed camera in the visible range. The set-up consists of an Olympus I-speed 3 camera mounting a SIGMA 105 mm macro lens, with a sampling frequency of 300 Hz. The spatial resolution was about 150 µm/pixel with a field of view of about 60x60 mm. Grasso *et al*. (2016) showed that the high-speed imaging in the visible range allows determining the local pixel intensity profile as a proxy of the local temperature profile, to be used for over-heating defect detection during the slice development.

In EBM, only off-axis monitoring systems are feasible. In this case, two set-ups are made possible by the existence of two viewports in Arcam EBM systems. One is analogous to the one used by many authors in SLM (e.g., Krauss *et al*., 2012, Moylan *et al*., 2014a, Lane *et al*., 2015 and Grasso *et al*., 2016), with the camera outside the front door window of the building chamber. This set-up was used by Gong et al. (2013b) and Price *et al*. (2012). These authors used the same NIR camera (780 - 1080 nm) with maximum frame rate of 60 Hz to capture 2D temperature profiles along the scan path and over the melt pool (field of view of 31x23 mm and resolution of about 48 µm/pixel). Other authors (Schwerdtfeger *et al*., 2012; Ridwan *et al*., 2014; Rodriguez *et al*., 2012 – 2015; Mireles *et al*., 2015; Dinwiddie *et al*., 2013) used the second viewport on the top of the chamber, close to the beam column. This second set-up allows a small mounting angle from the vertical axis, which provides a quasi-coaxial point-of-view of the entire powder bed with different resolutions (e.g., 830 µm/pixel in Schwerdtfeger *et al*., 2012, 350 µm/pixel in Rodriguez *et al*., 2012 – 2015) (Fig. 10).

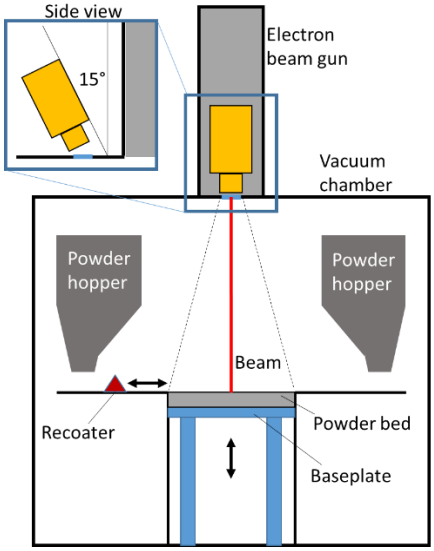

Fig. 10 – Off-axial monitoring set-up of EBM processes by using the viewport on the top of the build chamber (re-edited from Schwerdtfeger *et al*., 2012)

Table 5 – Main set-up parameters and setting proposed by authors for off-axial monitoring of EBM processes

Reference	Camera type	Wavelength range	Field of view	Lens and filters	Frame rate	Spatial resolution
Gong et al., 2013b	LumaSense MSC640 NIR camera	780 – 1080 nm	31x23 mm	Lens with 500 mm working distance	Max 60 Hz	46.8 µm/pixel (horizontally), 66.2 µm/pixel (vertically)
Price et al., 2012	LumaSense MSC640 NIR camera	780 – 1080 nm	31x23 mm (Lens A) 5.3x4.0 mm (Lens B)	Lens with (A) 500 mm work. dist. and (B) 350 mm work. dist.	Max 60 Hz	47.6 µm/pixel (lens A) 8.3 µm/pixel (lens B)
Schwerdtfeger et al., 2012	FLIR A320 IR camera	Unspecified	Entire build area	Unspecified	Not relevant to the application	830 µm/pixel
Ridwan et al., 2014	FLIR SC645 IR camera	Unspecified	Entire build area	Unspecified	Not relevant to the application	Unspecified
Rodriguez et al., 2012 - 2015	FLIR SC645 IR camera	Unspecified	Entire build area	Default 25° lens	Not relevant to the application	350 µm/pixel
Mireles et al., 2015	FLIR SC645 IR camera	Unspecified	Entire build area	Unspecified	Not relevant to the application	Unspecified
Dinwiddie et al., 2013	FLIR SC-8200 IR camera	Midwave IR range	Entire build area	Unfiltered 50 mm lens	Not relevant to the application	Unspecified

In all the reviewed studies, an IR camera was used, though for different monitoring purposes. Schwerdtfeger *et al*. (2012) used IR vision to characterize the surface pattern of scanned slices to detect flaws and surface defects. Analogously, Ridwan *et al*. (2014) and Mireles *et al*. (2015) used IR vision for surface pattern and geometry characterization of molten slices, whereas the temperature distribution over the entire build area was studied by Rodriguez *et al*. (2012 – 2015) and Mireles *et al*. (2015). The window metallization problem

caused by free metal ions and possible countermeasures were discussed by Dinwiddie *et al*. (2013) and Schwerdtfeger *et al*. (2012). Apart from the studies of Gong *et al*. (2013b) and Price *et al*. (2012), all other studied in EBM process monitoring focused on the analysis of the slice pattern, geometry and temperature distribution, which implies image acquisition to be performed at the end each layer. Table 5 summarizes the main set-up parameters proposed by different authors in EBM.

3.2.3. Other in-situ sensing systems

Other in-situ sensing approaches were proposed in the literature. Kleszczynski *et al*. (2014) and Reinarz and Witt (2012) investigated the use of an **accelerometer** mounted on the recoating system to measure its vibration during the powder deposition in SLM. As mentioned above, super-elevated edges may interfere with the deposition operation, leading to a fast increase of the recoater wear. Kleszczynski *et al*. (2014) studied the correlation between acceleration measurements and image-based super-elevated edge analysis, showing that a coupled use of these two in-situ information sources is suitable for detection of superelevated edges and possible recoater wear. Zur Jacobsmühlen *et al*. (2015) studied the same correlation to determine an acceleration value corresponding to critical super-elevated heights (see also Section 4). Rieder *et al*. (2014) proposed an **ultrasonic monitoring device** in SLM. An ultrasonic transducer (unfocused 10 MHz normal incidence probe of 6.3 mm) was mounted at the lowed side of the baseplate. The bandwidth range was 400 kHz up to 30 MHz, with an acquisition frequency of 250 mega-samples per second. Rieder *et al*. (2014) showed preliminary results suggesting that the proposed approach might provide qualitative in-process information about residual stresses and part porosity. Dunbar (2016) proposed an apparatus for in-situ measurement of the distortion of the part during the layer-wise process. Distortion measurements were performed using a Lord Microstrain differential variable reluctance transducer (DVRT) **displacement sensor** attached to the underside of the baseplate. In addition, the temperature of the baseplate was measured using K-Type **thermocouples**. Such an equipment allowed Dunbar (2016) to investigate the effect of scanning strategies on the build distortions.

Other authors studied non-destructive inspection techniques suitable for metal AM discussing their possible usage for in-situ measurements. As an example, Guan *et al*. (2015 – 2016) studied the **optical coherence tomography** (OCT) technique to capture cross-sectional structural images of the part in order to characterize the surface and sub-surface part integrity. Guan *et al*. (2015 – 2016) pointed out the OCT devices could be integrated in laser-based PBF systems for in-situ monitoring. Indeed, the rapid development of optical sensor and computing technology enables real-time monitoring and control. One solution suggested by Guan *et al*. (2015 – 2016) consists of combining OCT with other detectors, e.g., high-speed cameras, to perform a rough scan. Once the area of interest has been located, the OCT can apply a higher resolution scan and provide a higher-detail evaluation of the sub-surface. Smith *et al*. (2016) studied the spatially resolved acoustic spectroscopy technique for part inspection in SLM applications. The technique can be used to investigate the process parameter effect on the part quality and for the internal and sub-surface porosity characterization.

Smith *et al*. (2016) discussed the possibility of an in-situ implementation suggesting a possible co-axial integration of the instrument in SLM systems.

4. IN-PROCESS FAULT DETECTION AND CONTROL

The PBF process monitoring literature is still in a preliminary stage if compared to the corresponding literature in other production fields. As a matter of fact, most of the already mentioned studies were aimed at demonstrating the capability of measuring relevant quantities and signatures during the PBF process, and studying the effect of different parameters on those measured quantities. Indeed, the term "monitoring" is used in the mainstream literature cited in this study to indicate the in-situ data collection and feature extraction methodologies. Instead, from a statistical monitoring perspective, the term "monitoring" refers not only to the data collection but also to the detection of defects and faults via automated alarm rules. This latter kind of monitoring is needed to actually enhance the intelligent capabilities of next-generation PBF systems. Only few authors proposed automated rules and analytical methods for in-process defect detection. In addition, very few authors proposed control strategies to implement corrective or reactive actions once a defects has been detected. The following subsections briefly review these studies.

4.1. Melt pool monitoring

Regarding the melt pool signature monitoring, Clijsters *et al*. (2014) proposed a method to detect anomalous area and intensity values during the SLM of metal parts. The melt pool area and intensity were acquired by means of the co-axial sensing set-up described in Section 3.2. Clijsters *et al*. (2014) proposed the acquisition of melt pool area and intensity values along different scanned vectors. Those data are then classified depending on the local measured quality in terms of geometrical accuracy and roughness. The result is an estimation of confidence intervals for melt pool area and intensity based on scanned vectors that were classified as representative of an in-control process. In particular, two sets of confidence intervals were estimated, one for melt pools along internal filled hatches and one for melt pools along the slice contours. The monitoring tool proposed by Clijsters *et al*. (2014) works by comparing newly acquired melt pool area and intensity values to those limits, signalling outlying observations. Being known the spatial location of each observation within the building area, a defect detection in both time and space is made possible. Clijsters *et al*. (2014) demonstrated the capability of detecting both overheating phenomena at the edges of the part and internal defects. Fig. 11 shows the values of melt pool area acquired along a scan track compared with the reference confidence interval (Fig. 11, left panel), and an example of the local porosity caused by the over-heating effect in the beginning of the track (Fig. 11, right panel).

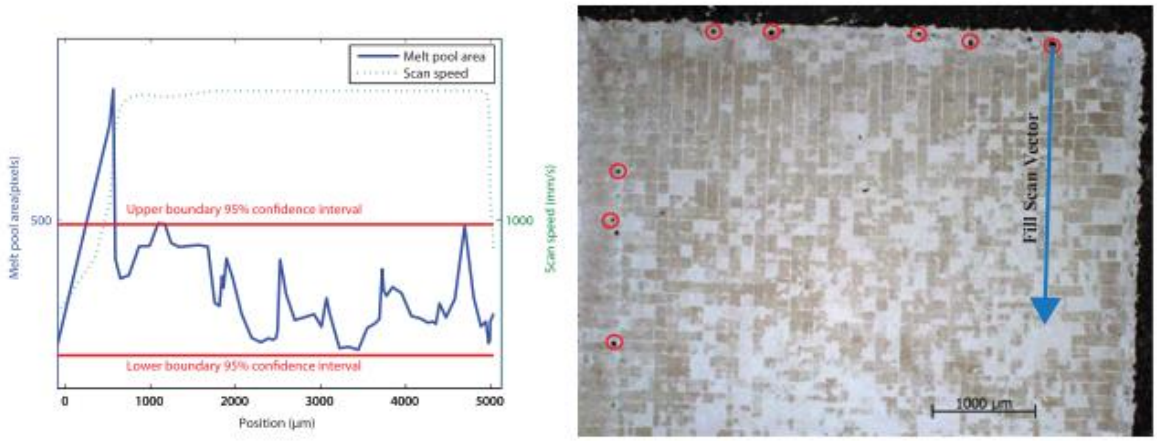

Fig. 11 – Melt pool area values of fill laser scan of a Ti6Al4V cube with high power (left) and local pores (black spots highlighted by the red circles) resulting from over-heating effects in the beginning of the fill vector (right) (Clijsters *et al*., 2014)

Kruth *et al*. (2007) and Craeghs *et al*. (2010) proposed a feedback control method in SLM where the observed process variable is the melt pool area, and the controlled parameter is the laser power. The melt pool area was measured either via a co-axial pyrometer (being the pyrometer signal proportional to the melt pool area, Craeghs *et al*., 2010) or a co-axial IR camera. A PID controller acts on the difference between the observed area and a reference setpoint. Kruth *et al*. (2007) states that such a setpoint needs to be determined experimentally for every different set of process parameters. Craeghs *et al*. (2010) experimentally determined the dynamic relation between the laser power and the photodiode signal (proxy of the melt pool area) as a second order model. Based on this dynamic relation Craeghs *et al*. (2010) designed a feedback PI controller with optimal bandwidth. The results of both Kruth *et al*. (2007) and Craeghs *et al*. (2010) show that the feedback control method allows improving the geometrical accuracy of overhang regions. Craeghs *et al*. (2010) also demonstrated an improvement of the surface roughness during the SLM of cubes with small scan spacing.

4.2. Track monitoring along the scan path

The monitoring of the track has been studied by different authors (e.g., Krauss *et al*., 2012 - 2014; Lane *et al*., 2015; Bayle and Doubenskaia, 2008; Schilp *et al*., 2014; Doubenskaia *et al*., 2015), but most of them focused on the analysis of effects of process parameters and scan strategies on the measured quantities.

Gong *et al*. (2013b), Thombansen *et al*. (2015) and Price *et al*. (2012) proposed a method to generate a spatial map of melt pool temperature acquired in different locations along the entire scan path. The result is a thermal homogeneity map of the entire slice. Such a representation enables the spatial localization of regions where an over-heating occurred, where geometrical errors and surface/internal defects are likely to be observed. Similarly, Kanko *et al*. (2016) showed a spatial mapping of melt pool morphological properties to

highlight regions of the scan path where deviations from the normal melting state occurred. Krauss *et al*. (2012) also studied the effect of artificial flaws on the shape of the irradiance profile and the thermogram acquired during the scanning of single tracks. Nevertheless, future research needs to include the development of automated rules for spatial defect classification and automated alarm generation.

A different perspective was proposed by Grasso *et al*. (2016). The underlying idea was to detect local over-heating phenomena along the scan path by analysing the intensity profile of each pixel. To this aim, Grasso *et al*. (2016) proposed the use of T-mode Principal Component Analysis (PCA) for image data to define a spatial statistical descriptor. The spatial mapping of the PCA-based descriptor allows identifying local "hot spots" that correspond to anomalous temporal correlation patterns observed in the pixel intensity profiles. These hot-spots were shown to correspond to regions of the scan path where a longer cooling-down transitory was caused by a wrong heat flux in correspondence of critical features (overhang structures and acute corners). Grasso *et al*. (2016) proposed an automated method based on k-means clustering applied to the spatial distribution of PCA-based descriptor for in-process defect detection. An adaptive updating of the clustering analysis allows detecting the generation of this kind of defects since their onset stage. The performances of the method were demonstrated in the production of complicated shapes in SLM. Fig. 12 shows an example of the automated spatial detection of an over-heating zone (red cluster) by recursively updating the clustering algorithm as successive video frames become available.

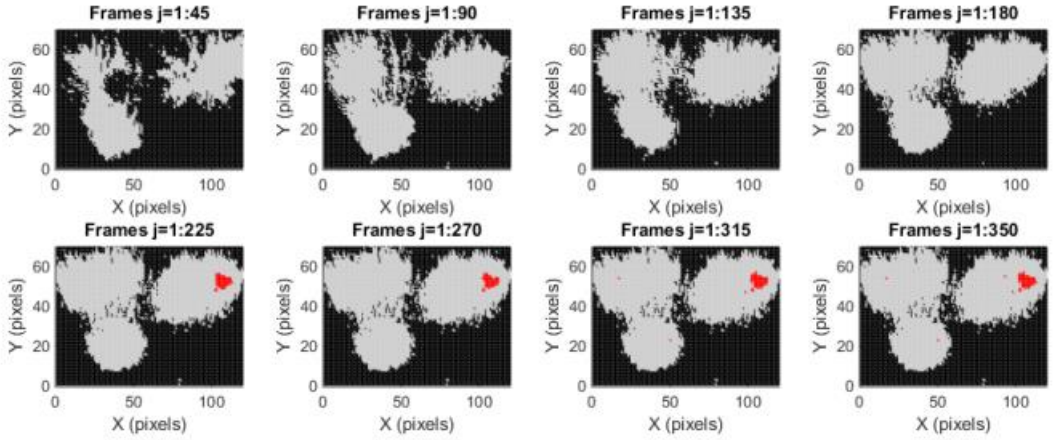

Fig. 12 – Example of spatial detection of the over-heating zone (red cluster) during the scan of one layer in SLM; different panels correspond to consecutive updating batches of processes video frames (Grasso *et al*., 2016)

4.3. Slice monitoring and geometry reconstruction

With regard to observable signatures at slice level, different authors applied image-processing techniques to segment the in-situ acquired images for three main purposes: i) the characterization of surface patterns for defect detection, ii) the reconstruction of the slice geometry for all the monitored layers and iii) the quantification of geometrical accuracy in terms of deviation from the nominal dimensions. Ridwan *et al*.

(2014) discussed the use of color image segmentation and edge detection algorithms in EBM to determine the boundaries of the slice and to estimate different descriptors, including the area and the perimeter. Then, the geometric accuracy was estimated as the difference between the observed values and the nominal ones available from the CAD and slicing software. Ridwan *et al*. (2014) showed that an indication of internal porosity is also suitable by means of this image-processing approach, in terms of segmented regions within the slice area. Foster *et al*. (2015) showed examples of 3D reconstructions of builds via image segmentation and slice edge detection. Although the details of the image processing algorithms were not provided, the presented examples highlighted the importance of this kind of analysis to detect when (in time) and where (in space) defects originated within the part. Zur Jacobsmühlen *et al*. (2015) proposed a thresholding method coupled with other post-process image adjusting operations to segment the images captured at the end of each layer via a high-resolution off-axis camera in the visible range. The goal was to detect super-elevated edges by comparing the monitored descriptor against an empirical threshold. The descriptor was defined as the product of the area and mean intensity of the examined region. Every region whose descriptor is higher than the threshold is classified as "critical" and signalled by the algorithm. Zur Jacobsmühlen *et al*. (2015) extended the previous study. In zur Jacobsmühlen *et al*. (2015), one threshold was set at three times the standard deviation of all the pixel intensities, and it was used to identify super-elevated areas. A second threshold was used to classify super-elevated areas as either critical or non-critical. The proposed approach involved the estimation of different descriptors, including the relative super-elevated area and the number of detected elevated regions. Both 2D and 3D mappings of the spatial locations of pixels corresponding to super-elevated areas were proposed to visualize the regions of the produced parts were this kind of defect was detected in-situ (Fig. 13). The availability of a threshold to classify the region as a critical elevated area enables the implementation of an alarm rule. This threshold was based on an experimental analysis were both image data and acceleration measures from an accelerometer mounted on the recoater were collected. The critical area threshold was linked to an experimentally determined acceleration value (zur Jacobsmühlen *et al*., 2015).

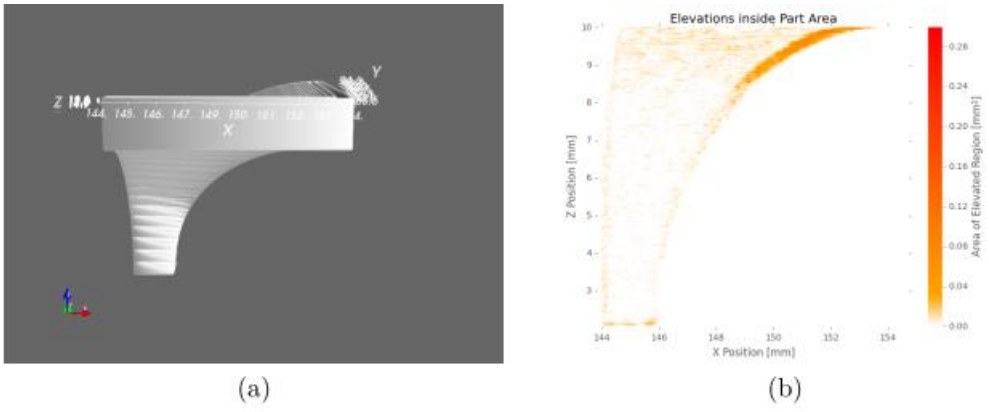

Fig. 13 – Geometry of the monitored part with decreasing overhang angle for increasing z (a) and x/z plot of elevated area locations and severity (zur Jacobsmühlen *et al*., 2015)

Schilp *et al*. (2014) proposed a defect indicator based on the evaluation of the temperature profile of each pixel belonging to the slice. The indicator consists of the total time the local temperature stayed above a certain temperature. Schilp *et al*. (2014) showed the generation of 2D and 3D spatial maps of this descriptor as a graphical means to detect the location of defects within each layer and within the entire part. A similar mapping based on an extension of the indicators of interest was proposed by Krauss *et al*. (2014). Indeed, Krauss *et al*. (2014) proposed evaluating the local maximum temperature and the cool-down behaviour in terms of a characteristic time as well. A spatial mapping of local slice heights was discussed by different authors (Zhang *et al*., 2016; Neef *et al*., 2014; Land *et al*., 2015). In this case, a threshold for the maximum allowed height might be defined and used to automatically signal the occurrence of super-elevated edges.

Mireles *et al*. (2015b) included a methodology similar to the one presented by Ridwan *et al*. (2014) into an automated process stopping rule in EBM. The proposed approach includes an estimation of internal porosity based on image thresholding and an estimation of the slice temperature. Both the porosity descriptor and the measured temperature are compared against upper and lower limits pre-defined by the user. If the in-situ measured values violate those limits, the build is automatically stopped. Mireles *et al*. (2015b) also discussed the possibility of stabilizing the microstructure of the part to obtain an isotropic grain size throughout the build by controlling the layer heating time. Mireles *et al.* (2015a) studied the possibility of in-situ defect correction by re-melting the affected area. This approach was tested by producing a part with seeded defects and evaluating the benefits of the re-melting operation. Mireles *et al.* (2015a) pointed out that this approach can be included into a closed-loop control strategy where the system is instructed to re-scan the affected region once the defect has been detected via thermal image acquisition at the end of each slice. Seeded defects consisted of artificial pores of different size (from 100 μm to 2000 μm) and different shape. The re-melting operation was found to correct all the seeded defects. The use of re-melting after each layer or only on the top surfaces in SLM was investigated by Yasa *et al*. (2011) as well. Yasa *et al*. (2011) showed that the re-melting operation improves the surface finishing of outer surfaces and, at the same time, the internal density. The suitability of re-melting to repair defects of metal parts in SLM and the benfits in terms of microstructure, local stress concentration, surface roughness and porosity correction were investigated by other studies (Grum and Slabe, 2006). Yasa *et al*. (2011) also discussed the combination of SLM and selective laser erosion (SLE), i.e., a subtractive process based on material evaporation. Yasa *et al*. (2011) pointed out four possible applications of the SLE: i) improvement of the surface quality and mitigation of super-elevated edges at the end of each layer, ii) improvement of the process resolution along the building direction by reducing the effective layer thickness before applying the next layer, iii) improvement of the surface roughness on the top (outer) surface, and iv) machining of small features to improve the in-layer accuracy. Yasa *et al*. (2011) showed an example of the use of SLE for this latter kind of application,

demonstrating the capability of producing inner and outer features having dimensions in the range 50 µm – 100 µm.

4.4. Powder bed monitoring

In powder bed monitoring, one major goal consists of detecting local inhomogeneities that may have a detrimental effect of the part quality. Foster *et al*. (2015) used an image-processing approach not only for the edge detection of the slice but also for the detection of local powder bed defects. In addition, Foster *et al*. (2015) showed a 3D reconstruction of the part based on in-situ images where the spatial location of powder bed defects was mapped as well. These defects included unfused particles dragged across the bed and irregularities caused by a bouncing effect of the recoated (Fig. 14). A topographic reconstruction of the powder bed was proposed by other authors (Neef *et al*., 2014; Erler *et al*., 2014). In principle, the in-process detection of powder bed defects can be used to activate corrective actions, like a re-deposition of the powder bed and/or, when possible, the substitution of a worn recoating system.

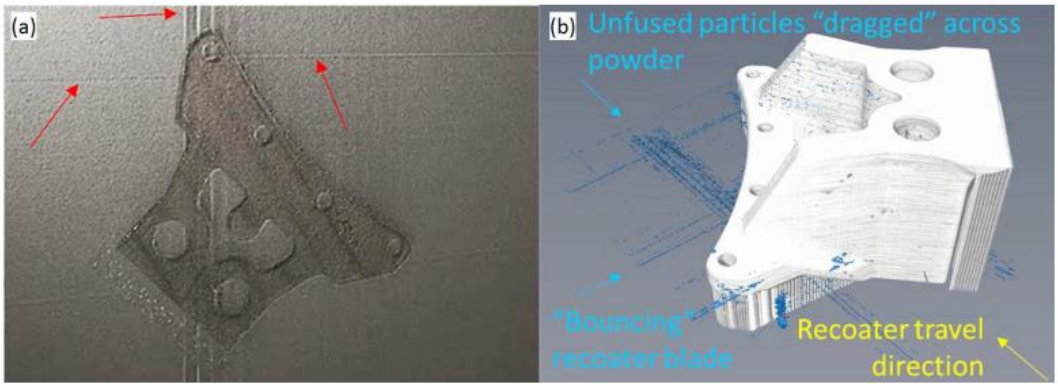

Fig. 14 – Example of image showing powder bed inhomogeneities (a) and 3D reconstruction of the produced part based on in-situ images, with the spatial mapping of powder bed defects (b) (Foster *et al*., 2015)

4.5. Other monitoring studies

Some authors proposed the use of vibration analysis of the recoating system to signal in-process alarms. In Section 4.3 the use of acceleration data to classify super-elevated regions as either critical or not was discussed (Zur Jacobsmühlen *et al*., 2015). Another study, authored by Reinarz and Witt (2012) proposed the use of acceleration measurements to detect the contact between the recoating system and the super-elevated regions of the slice. Reinarz and Witt (2012) proposed an experimental threshold for the acceleration that could be used to interrupt the process to avoid an undesired increase of the recoater wear with consequent defect inflation and propagation.

4.6. Commercial tools for in-situ sensing and data collection

Different PBF system developers (EOS, Concept Laser, Arcam, SLM Solutions) and third party equipment developers (B6 Sigma, Inc) offer process monitoring modules and toolkits. Most of them are mainly used to

collect data via in-situ sensing and provide the user with some post-process data reporting. Further development efforts are needed to implement analytical tools able to quickly make sense of gathered data during the process and automatically generate alarms. Table 6 summarizes some of these commercial toolkits.

Concept Laser developed a suite of monitoring tools that includes QM meltpool3D module (Concept Laser, 2016). QM meltpool3D relies on a co-axial monitoring set-up used to estimate the melt pool area and the intensity of process emissions from the melt pool region. The monitoring module provides two kinds of information. First, the averaged area and intensity values per component (when multiple parts are produced in the same build) and per layer are provided. Second, location-related area and intensity values are mapped onto the slice in order to generate a 3D dataset of the part and its structure. The QM meltpool3D module provides the data directly after the build process and is not currently used for defect correction or feedback control during the process. The QM-System suite developed by Concept Laser includes another module, called QM coating (Concept Laser, 2016), focused on the monitoring and control of the powder dose factor. The dose factor is the parameter that controls the amount of powder released by the powder hopper before the recoating operation. Depending on whether sufficient powder was applied, the powder dose factor is increased, reduced or a new coating is applied.

Table 6 – Commercial toolkits for PBF process monitoring[2]

Process	Toolkit name	Developer	Monitored signature	In-situ sensing
SLM	QM meltpool 3D	Concept Laser	Melt pool (area and intensity)	Co-axial camera and photodiode
	QM coating	Concept Laser	Powder bed	Off-axial camera
	EOSTATE MeltPool	EOS	Melt pool	Co-axial and off-axial sensors
	EOSTATE PowderBed	EOS	Powder bed	Off-axial camera
	PrintRite3D	B6 Sigma, Inc.	Different monitoring possibilities	Set of co-axial and off-axial sensors available
	Melt Pool Monitoring (MPM) system	SLM Solutions	Melt pool	Co-axial pyrometer
	Layer Control System (LCS)	SLM Solutions	Powder bed	Off-axial camera
EBM	LayerQam	Arcam	Slice pattern and geometry	Off-axial camera

EOS developed the EOSTATE MeltPool jointly with Plasmo Industrietechnik (EOS, 2016), as an extension to the EOS M290 DMLS system for monitoring the process. The light emitted by the melt pool region is measured and mapped onto the slice and the entire build. This allows determining the presence of local regions where the intensity was higher than the expected one. Also in this case, no in-process defect detection is currently available. EOS developed a module for the powder bed monitoring, too, called EOSTATE PowderBed. It exploits an integrated camera and optimised illumination to capture images of the powder

[2] Most performance details (e.g., frame rates, spatial resolutions, fields of view, etc.) are not made available in the time when this review is written.

bed uniformity. Bamberg *et al*. (2016) presented an in-situ monitoring equipment (based on a high resolution CMOS camera) to be commercialized by EOS that allows performing optical tomography of produced parts. The method is suitable for 3D geometric reconstruction and spatial localization of defects (e.g., lack-of-fusion areas). Monitoring solutions for both melt pool monitoring and powder bed monitoring were developed by SLM Solutions as well (SLM Solutions, 2016). The monitoring solutions are called Melt Pool Monitoring (MPM) systems and Layer Control system, respectively. The powder bed monitoring system is able to detect non-homogeneous depositions and automatically activate new recoating operations.

Arcam developed the LayerQam tool for defect detection, which exploits a high-resolution camera to monitor the process by capturing images every layer. The system is used to provide a report at the end of the process about observed patterns. Analogous embedded sensing solutions for in-situ data collection have been installed by other PBF system developers (e.g., Renishaw, 2016) on their new products or are currently under development. However, further research efforts are needed to pass from a simple post-process reporting about measured quantities to the implementation of actual in-process monitoring and fault detection tools.

In addition to the toolkits developed by PBF system developed, a third party in-process quality assurance toolkit for metal AM processes was developed by B6 Sigma, Inc.. The suite is called PrintRite 3D and includes four modules: PrintRite 3D Sensorpak is a set of off-the-shelf co-axial and off-axial sensors that can be installed into the system. PrintRite 3D Inspect is a software for part inspection based on in-process data. It uses in-situ sensor data to determine quality metrics and to identify suspect patterns on a layer-by-layer basis. PrintRite 3D Contour is a software for real-time monitoring and reconstruction of the part geometry, and for comparisons with the CAD model. Another module for data analytics is currently under development.

It is worth noting that the current lack of "open systems" makes third party development of process monitoring and/or control tools for PBF systems very challenging. Nevertheless, there are ongoing efforts to develop an "Open Communication Protocol" for open communications of real-time and position-synchronized sensor data (Dunbar *et al.*, 2016).

5. CONCLUSIONS

There is a rapidly increasing number of studies in the literature aimed at understanding the nature and the source of defects in PBF processes, their effects on the product quality and how they can be mitigated or avoided by acting on several controllable parameters. Indeed, the lack of robustness and stability of metal AM processes, and of PBF processes in particular, has been widely pointed out as one major issue that deserves considerable research efforts and technological advances. The development and implementation of in-situ monitoring and control solutions represents a priority to push forward the industrial breakthrough of metal AM systems. In-situ sensing has been proposed for different observable signatures, including the

melt pool, the track along the scan path, the slice and the powder bed. A few authors showed that other quantities are measurable as well, including the recoating system vibration, the part and baseplate distortion, and the acoustic emissions of the process. The largest portion of the literature considered the use of imaging systems and non-contact temperature measurements (including pyrometers and IR cameras). In some cases, fringe projection and low-coherence interferometric techniques were proposed for local topography reconstruction. Other in situ non destructive inspection systems are currently under development, e.g., optical coherence tomography, and may be implemented and tested in the near future.

Different challenges must be faced for an extensive adoption of in-situ sensing in industry. One challenge regards the calibration of sensors, with particular reference to non-contact temperature measurements and machine vision. Another challenge regards the data management. Big data streams at high frequency are generated during an entire building process, and hence data dimensionality reduction techniques are expected to play a relevant role in the development of process monitoring tools. On the other hand, suitable data infrastructures must be adopted, possibly based on networked systems and centralized servers for data storage and analysis. Major research efforts are needed to develop and implement data mining and analysis methods for automated defect detection, in a statistical process monitoring framework. In particular, there is the need for statistical monitoring methods able to cope with the natural variability of observed quantities, together with their spatial or spatio-temporal properties, and to design reliable alarm rules. This implies facing different issues. First, the one-of-a-kind and highly customized nature of many PBF applications prevents from the use of historic samples collected under normal (in-control) process conditions for the training of monitoring tools. Second, the very high sampling frequency for melt pool and track monitoring, together with the large dimensionality of the acquired data makes real-time analysis a challenging task that motivates the study of novel and computationally efficient methodologies.

Regarding the development of either reactive, corrective or feedback control actions, very few seminal studies have been published so far. In some cases, an in-process adaptation of the laser power based on observed melt pool properties was proposed. Other studies discussed the automated interruption of the process when monitored quantities violate certain thresholds. The possibility of defect repairing was proposed as well. In particular, both in-situ laser re-melting and selective laser erosion technique were shown to be feasible to mitigate different kinds of defects and to enhance the quality of the final part. Currently, the closed nature of some PBF systems and their controller imposed some limitations to the research in this field. However, in-process detection of defects and feedback control methods are expected to experience a substantial step forward in the next few years because of an increasing industrial pull for these technologies.

Acknowledgments

The study was partially funded by the AMATHO Project-Additive MAnufacturing for Tiltrotor HOusing- under H2020-EU.3.4.5.3.-IADP Fast Rotorcraft, in the frame of the CleanSky2-IA Programme, and by the National Technology Cluster project "CTN01_00163_216758–High Performance Manufacturing", funded by the Italian Ministry of Education, University and Research.

REFERENCES

Advanced Powders, http://advancedpowders.com (last access: 02/11/2016)

Ardila, L. C., Garciandia, F., González-Díaz, J. B., Álvarez, P., Echeverria, A., Petite, M. M., ... & Ochoa, J. (2014). Effect of IN718 recycled powder reuse on properties of parts manufactured by means of selective laser melting. Physics Procedia, 56, 99-107.

Arısoy, Y. M., Criales, L. E., Özel, T., Lane, B., Moylan, S., & Donmez, A. (2016). Influence of scan strategy and process parameters on microstructure and its optimization in additively manufactured nickel alloy 625 via laser powder bed fusion. *The International Journal of Advanced Manufacturing Technology*, 1-25.

Attar, E. (2011). Simulation of selective electron beam melting processes. *PhD Dissertation, Technischen Fakultat der Universitat Erlangen-Nurnberg*

Aziz, M. S. A., Furumoto, T., Kuriyama, K., Takago, S., Abe, S., Hosokawa, A., & Ueda, T. (2013). Residual stress and deformation of consolidated structure obtained by layered manufacturing process. *Journal of Advanced Mechanical Design, Systems, and Manufacturing*, *7*(2), 244-256.

Bamberg, J., Zenzinger, G., Ladewig, A. (2016). In-process control of selective laser melting by quantitative optical tomography, 19th World Conference on Non-Destructive Testing, 2016

Bayle, F., & Doubenskaia, M. (2008, January). Selective laser melting process monitoring with high speed infra-red camera and pyrometer. In *Fundamentals of Laser Assisted Micro-and Nanotechnologies* (pp. 698505-698505). International Society for Optics and Photonics.

Berumen, S., Bechmann, F., Lindner, S., Kruth, J. P., & Craeghs, T. (2010). Quality control of laser-and powder bed-based Additive Manufacturing (AM) technologies. *Physics procedia*, *5*, 617-622.

Bi, G., Sun, C. N., & Gasser, A. (2013). Study on influential factors for process monitoring and control in laser aided additive manufacturing. *Journal of Materials Processing Technology*, *213*(3), 463-468.

Biamino S.; Penna A. ; Ackelid U.; Sabbadini S.; Tassa O.; Fino P.; Pavese M.; Gennaro P.; Badini C. (2011), Electron beam melting of Tie48Ale2Cre2Nb alloy: Microstructure and mechanical properties investigation, *Intermetallics 19*, 776-781

Buchbinder, D., Meiners, W., Pirch, N., Wissenbach, K., & Schrage, J. (2014). Investigation on reducing distortion by preheating during manufacture of aluminum components using selective laser melting. *Journal of Laser Applications*, *26*(1), 012004.

Carter, L. N., Attallah, M. M., & Reed, R. C. (2012). Laser powder bed fabrication of nickel-base superalloys: influence of parameters; characterisation, quantification and mitigation of cracking. *Superalloys 2012*, 577-586.

Carter, L. N., Martin, C., Withers, P. J., & Attallah, M. M. (2014). The influence of the laser scan strategy on grain structure and cracking behaviour in SLM powder-bed fabricated nickel superalloy. *Journal of Alloys and Compounds*, *615*, 338-347.

Casati, R., Lemke, J., & Vedani, M. (2016). Microstructure and Fracture Behavior of 316L Austenitic Stainless Steel Produced by Selective Laser Melting. *Journal of Materials Science & Technology*, *32*(8), 738-744.

Casavola, C., Campanelli, S. L., & Pappalettere, C. (2008, June). Experimental analysis of residual stresses in the selective laser melting process. In *Proccedings of the XIth International Congress and Exposition, Orlando, Florida, USA*.

Cheng, B., Shrestha, S., & Chou, K. (2016). Stress and deformation evaluations of scanning strategy effect in selective laser melting. *Additive Manufacturing*.

Chivel, Y. (2013). Optical in-process temperature monitoring of selective laser melting. *Physics Procedia*, *41*, 904-910.

Chlebus, E., Kuźnicka, B., Kurzynowski, T., & Dybała, B. (2011). Microstructure and mechanical behaviour of Ti—6Al—7Nb alloy produced by selective laser melting. *Materials Characterization*, *62*(5), 488-495.

Clijsters, S., Craeghs, T., Buls, S., Kempen, K., & Kruth, J. P. (2014). In situ quality control of the selective laser melting process using a high-speed, real-time melt pool monitoring system. *The International Journal of Advanced Manufacturing Technology*, *75*(5-8), 1089-1101.

Concept Laser http://www.conceptlaserinc.com/in-situ-quality-assurance-with-qmmeltpool-3d-from-concept-laser (last access: 3/11/2016)

Craeghs, T., Bechmann, F., Berumen, S., & Kruth, J. P. (2010). Feedback control of Layerwise Laser Melting using optical sensors. *Physics Procedia*, *5*, 505-514.

Craeghs, T., Clijsters, S., Kruth, J. P., Bechmann, F., & Ebert, M. C. (2012). Detection of process failures in layerwise laser melting with optical process monitoring. *Physics Procedia*, *39*, 753-759.

Craeghs, T., Clijsters, S., Yasa, E., Bechmann, F., Berumen, S., & Kruth, J. P. (2011). Determination of geometrical factors in Layerwise Laser Melting using optical process monitoring. *Optics and Lasers in Engineering*, *49*(12), 1440-1446.

Das, S. (2003). Physical aspects of process control in selective laser sintering of metals. *Advanced Engineering Materials*, *5*(10), 701-711.

Delgado, J., Ciurana, J., & Rodríguez, C. A. (2012). Influence of process parameters on part quality and mechanical properties for DMLS and SLM with iron-based materials. *The International Journal of Advanced Manufacturing Technology*, *60*(5-8), 601-610.

Denlinger, E. R., Heigel, J. C., & Michaleris, P. (2014). Residual stress and distortion modeling of electron beam direct manufacturing Ti-6Al-4V. *Proceedings of the Institution of Mechanical Engineers, Part B: Journal of Engineering Manufacture*, 0954405414539494.

Dinwiddie, R. B., Dehoff, R. R., Lloyd, P. D., Lowe, L. E., & Ulrich, J. B. (2013, May). Thermographic in-situ process monitoring of the electron-beam melting technology used in additive manufacturing. In *SPIE Defense, Security, and Sensing* (pp. 87050K-87050K). International Society for Optics and Photonics.

Doubenskaia, M. A., Zhirnov, I. V., Teleshevskiy, V. I., Bertrand, P., & Smurov, I. Y. (2015). Determination of true temperature in selective laser melting of metal powder using infrared camera. In *Materials Science Forum* (Vol. 834, pp. 93-102). Trans Tech Publications.

Doubenskaia, M., Grigoriev, S., Zhirnov, I., & Smurov, I. (2016). Parametric analysis of SLM using comprehensive optical monitoring. *Rapid Prototyping Journal*, *22*(1), 40-50.

Doubenskaia, M., Pavlov, M., Grigoriev, S., Tikhonova, E., & Smurov, I. (2012). Comprehensive optical monitoring of selective laser melting. *Journal of Laser Micro Nanoengineering*, *7*(3), 236-243.

Dunbar, A. J. (2016). *Analysis of the Laser Powder Bed Fusion Additive Manufacturing Process Through Experimental Measurement and Finite Element Modeling* (Doctoral dissertation, The Pennsylvania State University).

Dunbar, A.J., Nassar, A.R., Reutzel, E.W., Blecher, J.J. A real-time communication architecture for metal powder bed fusion additive manufacturing, Proceedings of the 27th Annual Solid Freeform Fabrication Symposium, 67-80, 8-10 Aug 2016, Austin, TX, USA

Dye, D., Hunziker, O., & Reed, R. C. (2001). Numerical analysis of the weldability of superalloys. *Acta Materialia*, *49*(4), 683-697.

Edwards, P., O'Conner, A., & Ramulu, M. (2013). Electron beam additive manufacturing of titanium components: properties and performance. *Journal of Manufacturing Science and Engineering*, *135*(6), 061016.

EOS https://www.eos.info/software/dmls-meltpool-monitoring (last access: 3/11/2016)

Erler, M., Streek, A., Schulze, C., Exner, H. (2014). Novel machine and measurement concept for micro machining by Selective Laser Sintering, Solid Freeform Fabrication Symposium, 2014

Eschey, C., Lutzmann, S., & Zaeh, M. F. (2009). Examination of the powder spreading effect in Electron Beam Melting (EBM). *Solid Freeform Fabrication, Austin, TX, August*, 3-5.

Everton, S. K., Hirsch, M., Stravroulakis, P., Leach, R. K., & Clare, A. T. (2016). Review of in-situ process monitoring and in-situ metrology for metal additive manufacturing. *Materials & Design*, *95*, 431-445.

Ferrar, B., Mullen, L., Jones, E., Stamp, R., & Sutcliffe, C. J. (2012). Gas flow effects on selective laser melting (SLM) manufacturing performance. *Journal of Materials Processing Technology*, *212*(2), 355-364.

Foster, B. K., Reutzel, E. W., Nassar, A. R., Hall, B. T., Brown, S. W., & Dickman, C. J. (2015) Optical, layerwise monitoring of powder bed fusion. In *Solid Free. Fabr. Symp. Proc*, 295-307.

Fox, J. C., Moylan, S. P., & Lane, B. M. (2016). Effect of Process Parameters on the Surface Roughness of Overhanging Structures in Laser Powder Bed Fusion Additive Manufacturing. *Procedia CIRP*, *45*, 131-134.

Gibson, I., Rosen, D. W., Stucker, B. (2010). Additive manufacturing technologies. New York: Springer.

Gong, H., (2013) Generation and detection of defects in metallic parts fabricated by selective laser melting and electron beam melting and their effects on mechanical properties. *UofL Electronic Theses and Dissertations. Paper 515*.http://dx.doi.org/10.18297/etd/515

Gong, H., Rafi, K., Karthik, N., Starr, T., & Stucker, B. (2013a). Defect morphology in Ti–6Al–4V parts fabricated by selective laser melting and electron beam melting. In *24rd Annual International Solid Freeform Fabrication Symposium—An Additive Manufacturing Conference, Austin, TX, Aug* (pp. 12-14).

Gong, X., Cheng, B., Price, S., & Chou, K. (2013b). Powder-bed electron-beam-melting additive manufacturing: powder characterization, process simulation and metrology. In *Proceedings of the ASME District F Early Career Technical Conference* (pp. 59-66).

Grasso, M., Laguzza, V., Semeraro, Q., & Colosimo, B. M. (2016). In-process Monitoring of Selective Laser Melting: Spatial Detection of Defects via Image Data Analysis. Journal of Manufacturing Science and Engineering, 139(5), 051001-1 – 051001-16.

Grum, J., & Slabe, J. M. (2006). Effect of laser-remelting of surface cracks on microstructure and residual stresses in 12Ni maraging steel. *Applied Surface Science*, *252*(13), 4486-4492.

Gu, H., Gong, H., Pal, D., Rafi, K., Starr, T., & Stucker, B. (2013). Influences of energy density on porosity and microstructure of selective laser melted 17-4PH stainless steel. In *Proceedings of Solid Freeform Fabrication Symposium* (pp. 474-479).

Guan, G., Hirsch, M., Lu, Z. H., Childs, D. T., Matcher, S. J., Goodridge, R., ... & Clare, A. T. (2015). Evaluation of selective laser sintering processes by optical coherence tomography. *Materials & Design*, *88*, 837-846.

Guan, G., Hirsch, M., Syam, W. P., Leach, R. K., Huang, Z., & Clare, A. T. (2016, July). Loose powder detection and surface characterization in selective laser sintering via optical coherence tomography. In *Proc. R. Soc. A* (Vol. 472, No. 2191, p. 20160201). The Royal Society.

Hann, B. A. (2016). Powder Reuse and Its Effects on Laser Based Powder Fusion Additive Manufactured Alloy 718. SAE International Journal of Aerospace, 9(2016-01-2071).

Harrison, N. J., Todd, I., & Mumtaz, K. (2015). Reduction of micro-cracking in nickel superalloys processed by selective laser melting: a fundamental alloy design approach. *Acta Materialia*, *94*, 59-68.

Huang, Q., Hu, N., Yang, X., Zhang, R., & Feng, Q. (2016). Microstructure and inclusion of Ti–6Al–4V fabricated by selective laser melting. *Frontiers of Materials Science*, 1-4.

Irrinki, H., Dexter, M., Barmore, B., Enneti, R., Pasebani, S., Badwe, S., ... & Atre, S. V. (2016). Effects of Powder Attributes and Laser Powder Bed Fusion (L-PBF) Process Conditions on the Densification and Mechanical Properties of 17-4 PH Stainless Steel. *JOM*, *68*(3), 860-868.

Islam, M., Purtonen, T., Piili, H., Salminen, A., & Nyrhilä, O. (2013). Temperature profile and imaging analysis of laser additive manufacturing of stainless steel. *Physics Procedia*, *41*, 835-842.

ISO/ASTM 52900:2015(E), Standard Terminology for Additive Manufacturing – General Principles – Terminology (2015), www.astm.org

Kanko, J. A., Sibley, A. P., & Fraser, J. M. (2016). In situ morphology-based defect detection of selective laser melting through inline coherent imaging. *Journal of Materials Processing Technology*, *231*, 488-500.

Karlsson, J., Snis, A., Engqvist, H., & Lausmaa, J. (2013). Characterization and comparison of materials produced by Electron Beam Melting (EBM) of two different Ti–6Al–4V powder fractions. *Journal of Materials Processing Technology*, *213*(12), 2109-2118.

Kempen, K., Thijs, L., Vrancken, B., Buls, S., Van Humbeeck, J., & Kruth, J. P. (2013). Producing crack-free, high density M2 Hss parts by selective laser melting: pre-heating the baseplate. In *Proceedings of the 24th international solid freeform fabrication symposium. Laboratory for freeform fabrication, Austin, TX* (pp. 131-139).

Khairallah, S. A., Anderson, A. T., Rubenchik, A., & King, W. E. (2016). Laser powder-bed fusion additive manufacturing: Physics of complex melt flow and formation mechanisms of pores, spatter, and denudation zones. *Acta Materialia*, *108*, 36-45.

King, W. E., Barth, H. D., Castillo, V. M., Gallegos, G. F., Gibbs, J. W., Hahn, D. E., ... & Rubenchik, A. M. (2014). Observation of keyhole-mode laser melting in laser powder-bed fusion additive manufacturing. *Journal of Materials Processing Technology*, *214*(12), 2915-2925.

Kleszczynski, S., zur Jacobsmühlen, J., Reinarz, B., Sehrt, J. T., Witt, G., & Merhof, D. (2014). Improving process stability of laser beam melting systems. In *Proceedings of the Frauenhofer Direct Digital Manufacturing Conference*.

Kleszczynski, S., zur Jacobsmühlen, J., Sehrt, J. T., & Witt, G. (2012). Error detection in laser beam melting systems by high resolution imaging. In *Proceedings of the Solid Freeform Fabrication Symposium*.

Krauss, H., Eschey, C., & Zaeh, M. (2012, August). Thermography for monitoring the selective laser melting process. In *Proceedings of the Solid Freeform Fabrication Symposium*.

Krauss, H., Zeugner, T., & Zaeh, M. F. (2014). Layerwise monitoring of the selective laser melting process by thermography. *Physics Procedia*, *56*, 64-71.

Kruth, J. P., Badrossamay, M., Yasa, E., Deckers, J., Thijs, L., & Van Humbeeck, J. (2010). Part and material properties in selective laser melting of metals. In *Proceedings of the 16th international symposium on electromachining*.

Kruth, J. P., Froyen, L., Van Vaerenbergh, J., Mercelis, P., Rombouts, M., & Lauwers, B. (2004). Selective laser melting of iron-based powder. *Journal of Materials Processing Technology*, *149*(1), 616-622.

Kruth, J. P., Mercelis, P., Van Vaerenbergh, J., & Craeghs, T. (2007). Feedback control of selective laser melting. In *Proceedings of the 3rd international conference on advanced research in virtual and rapid prototyping* (pp. 521-527).

Kruth, J.P., Levy, G., Klocke, F., Childs, T.H.C., (2007). Consolidation phenomena in laser and powder-bed based layered manufacturing. CIRP Ann.—Manuf. Technol. 56, 730–759.

Land, W. S., Zhang, B., Ziegert, J., & Davies, A. (2015). In-situ metrology system for laser powder bed fusion additive process. *Procedia Manufacturing*, *1*, 393-403.

Lane, B., Moylan, S., Whitenton, E. P., & Ma, L. (2015). Thermographic Measurements of the Commercial Laser Powder Bed Fusion Process at NIST. In *Proc. Solid Free. Fabr. Symp* (Vol. 575).

Leuders, S., Thöne, M., Riemer, A., Niendorf, T., Tröster, T., Richard, H. A., & Maier, H. J. (2013). On the mechanical behaviour of titanium alloy TiAl6V4 manufactured by selective laser melting: Fatigue resistance and crack growth performance. *International Journal of Fatigue*, *48*, 300-307.

Li, R., Liu, J., Shi, Y., Wang, L., & Jiang, W. (2012). Balling behavior of stainless steel and nickel powder during selective laser melting process. *The International Journal of Advanced Manufacturing Technology*, *59*(9-12), 1025-1035.

Liu, B., Wildman, R., Tuck, C., Ashcroft, I., & Hague, R. (2011). Investigation the effect of particle size distribution on processing parameters optimisation in selective laser melting process. In *International solid freeform fabrication symposium: an additive manufacturing conference. University of Texas at Austin, Austin* (pp. 227-238).

Liu, Y., Yang, Y., Mai, S., Wang, D., & Song, C. (2015). Investigation into spatter behavior during selective laser melting of AISI 316L stainless steel powder. *Materials & Design*, *87*, 797-806.

Lott, P., Schleifenbaum, H., Meiners, W., Wissenbach, K., Hinke, C., & Bültmann, J. (2011). Design of an optical system for the in situ process monitoring of selective laser melting (SLM). *Physics Procedia*, *12*, 683-690.

Lu, S., Fujii, H., & Nogi, K. (2004). Sensitivity of Marangoni convection and weld shape variations to welding parameters in O 2–Ar shielded GTA welding. *Scripta Materialia*, *51*(3), 271-277.

Mahale, T. R. (2009). *Electron beam melting of advanced materials and structures*. PhD Dissertation, North Carolina State University

Mani, M., Lane, B., Donmez, A., Feng, S., Moylan, S., & Fesperman, R. (2015). Measurement science needs for real-time control of additive manufacturing powder bed fusion processes. *National Institute of Standards and Technology, Gaithersburg, MD, NIST Interagency/Internal Report (NISTIR)*, *8036*.

Matthews, M. J., Guss, G., Khairallah, S. A., Rubenchik, A. M., Depond, P. J., & King, W. E. (2016). Denudation of metal powder layers in laser powder bed fusion processes. *Acta Materialia*, *114*, 33-42.

Megahed, M., Mindt, H. W., N'Dri, N., Duan, H., & Desmaison, O. (2016). Metal additive-manufacturing process and residual stress modeling. *Integrating Materials and Manufacturing Innovation*, *5*(1), 1-33.

Meier, H., & Haberland, C. (2008). Experimental studies on selective laser melting of metallic parts. *Materialwissenschaft und Werkstofftechnik*, *39*(9), 665-670.

Mellor, S., Hao, L., Zhang, D. (2014). Additive manufacturing: A framework for implementation. International Journal of Production Economics, 149, 194-201.

Mercelis, P., & Kruth, J. P. (2006). Residual stresses in selective laser sintering and selective laser melting. *Rapid Prototyping Journal*, *12*(5), 254-265.

Mireles, J., Ridwan, S., Morton, P. A., Hinojos, A., & Wicker, R. B. (2015a). Analysis and correction of defects within parts fabricated using powder bed fusion technology. *Surface Topography: Metrology and Properties*, *3*(3), 034002.

Mireles, J., Terrazas, C., Gaytan, S. M., Roberson, D. A., & Wicker, R. B. (2015b). Closed-loop automatic feedback control in electron beam melting. *The International Journal of Advanced Manufacturing Technology*, *78*(5-8), 1193-1199.

Mousa, A.A. (2016). Experimental investigations of curling phenomenon in selective laser sintering process. *Rapid Prototyping Journal*, *22*(2), 405-415.

Mower, T. M., & Long, M. J. (2016). Mechanical behavior of additive manufactured, powder-bed laser-fused materials. *Materials Science and Engineering: A*, *651*, 198-213.

Moylan, S., Whitenton, E., Lane, B., & Slotwinski, J. (2014a). Infrared thermography for laser-based powder bed fusion additive manufacturing processes. In *AIP Conference Proceedings* (Vol. 1581, No. 1, pp. 1191-1196).

Moylan, S.P., Drescher, J., Donmez, M.A., (2014b) Powder bed fusion machine performance testing, Preceedings of the 2014 ASPE Spring Topical Meeting – Dimensional Accuracy and Surface Finish in Additive Manufacturing, 57, Berkeley, CA

Mumtaz, K. A., & Hopkinson, N. (2010). Selective laser melting of thin wall parts using pulse shaping. *Journal of Materials Processing Technology*, *210*(2), 279-287.

Neef, A., Seyda, V., Herzog, D., Emmelmann, C., Schönleber, M., & Kogel-Hollacher, M. (2014). Low coherence interferometry in selective laser melting. *Physics Procedia*, *56*, 82-89.

Niu, H. J., & Chang, I. T. H. (1999). Instability of scan tracks of selective laser sintering of high speed steel powder. *Scripta Materialia*, *41*(11), 1229-1234.

Olakanmi, E. O., Cochrane, R. F., & Dalgarno, K. W. (2015). A review on selective laser sintering/melting (SLS/SLM) of aluminium alloy powders: Processing, microstructure, and properties. *Progress in Materials Science*, *74*, 401-477.

Parry, L., Ashcroft, I. A., & Wildman, R. D. (2016). Understanding the effect of laser scan strategy on residual stress in selective laser melting through thermo-mechanical simulation. *Additive Manufacturing*.

Pavlov, M., Doubenskaia, M., & Smurov, I. (2010). Pyrometric analysis of thermal processes in SLM technology. *Physics Procedia*, *5*, 523-531.

Prabhakar, P., Sames, W. J., Dehoff, R., & Babu, S. S. (2015). Computational modeling of residual stress formation during the electron beam melting process for Inconel 718. *Additive Manufacturing*, *7*, 83-91.

Price, S., Cooper, K., & Chou, K. (2012). Evaluations of temperature measurements by near-infrared thermography in powder-based electron-beam additive manufacturing. In *Proceedings of the Solid Freeform Fabrication Symposium* (pp. 761-773). University of Texas, Austin, TX.

Price, S., Cheng, B., Lydon, J., Cooper, K., Chou, K. (2014). Temperature measurements in powder-bed electron beam additive manufacturing, Proc. of ASME International Mech Engr Congress and Exposition (IMECE2014), Nov 14-20, 2014, Montreal, Quebec, Canada.

Puebla, K., Murr, L. E., Gaytan, S. M., Martinez, E., Medina, F., & Wicker, R. B. (2012). Effect of melt scan rate on microstructure and macrostructure for electron beam melting of Ti-6Al-4V.

Rafi, H. K., Karthik, N. V., Gong, H., Starr, T. L., & Stucker, B. E. (2013). Microstructures and mechanical properties of Ti6Al4V parts fabricated by selective laser melting and electron beam melting. *Journal of materials engineering and performance*, *22*(12), 3872-3883.

Read, N., Wang, W., Essa, K., & Attallah, M. M. (2015). Selective laser melting of AlSi10Mg alloy: Process optimisation and mechanical properties development. *Materials & Design*, *65*, 417-424.

Reinarz, B., Witt, G. (2012), Process monitoring in the laser beam melting process – Reduction of process breakdowns and defective parts, Material Science & Technology Conference, 2012

Renishaw http://www.renishaw.com/en/additive-manufacturing-systems--15239 (last access: 3/11/2016)

Ridwan, S., Mireles, J., Gaytan, S. M., Espalin, D., & Wicker, R. B. (2014). Automatic layerwise acquisition of thermal and geometric data of the electron beam melting process using infrared thermography. In *Proc. Int. Symp. Solid Freeform Fabrication* (Vol. 343).

Rieder, H., Dillhöfer, A., Spies, M., Bamberg, J., & Hess, T. (2014, October). Online monitoring of additive manufacturing processes using ultrasound. In *Proceedings of the 11th European Conference on Non-Destructive Testing, October* (pp. 6-10).

Riemer, A., Leuders, S., Thöne, M., Richard, H. A., Tröster, T., & Niendorf, T. (2014). On the fatigue crack growth behavior in 316L stainless steel manufactured by selective laser melting. *Engineering Fracture Mechanics*, *120*, 15-25.

Rodriguez, E., Medina, F., Espalin, D., Terrazas, C., Muse, D., Henry, C., ... & Wicker, R. B. (2012, August). Integration of a thermal imaging feedback control system in electron beam melting. In *Proceedings of the Solid Freeform Fabrication Symposium*.

Rodriguez, E., Mireles, J., Terrazas, C. A., Espalin, D., Perez, M. A., & Wicker, R. B. (2015). Approximation of absolute surface temperature measurements of powder bed fusion additive manufacturing technology using in situ infrared thermography. *Additive Manufacturing*, *5*, 31-39.

Sames, W. J., List, F. A., Pannala, S., Dehoff, R. R., & Babu, S. S. (2016). The metallurgy and processing science of metal additive manufacturing. *International Materials Reviews*, 1-46.

Scharowsky, T., Juechter, V., Singer, R. F., & Körner, C. (2015). Influence of the scanning strategy on the microstructure and mechanical properties in selective electron beam melting of Ti–6Al–4V. *Advanced Engineering Materials*, *17*(11), 1573-1578.

Schilp, J., Seidel, C., Krauss, H., & Weirather, J. (2014). Investigations on temperature fields during laser beam melting by means of process monitoring and multiscale process modelling. *Advances in Mechanical Engineering*, *6*, 217584.

Schwerdtfeger, J., Singer, R. F., & Körner, C. (2012). In situ flaw detection by IR-imaging during electron beam melting. *Rapid Prototyping Journal*, *18*(4), 259-263.

Seifi, M., Salem, A., Beuth, J., Harrysson, O., & Lewandowski, J. J. (2016). Overview of materials qualification needs for metal additive manufacturing. *JOM*, *68*(3), 747-764.

Seyda, V., Kaufmann, N., & Emmelmann, C. (2012). Investigation of aging processes of Ti-6Al-4 V powder material in laser melting. *Physics Procedia*, *39*, 425-431.

Sharratt, B. M. (2015). Non-Destructive Techniques and Technologies for Qualification of Additive Manufactured Parts and Processes. A literature Review. *Contract Report DRDC-RDDC-2015-C035*, *Victoria, BC*.

SLM Solutions https://slm-solutions.com/products/machines/melt-pool-monitoring-mpm (last access: 3/11/2016)

Slotwinski, J. A., & Garboczi, E. J. (2014, February). Porosity of additive manufacturing parts for process monitoring. In *40TH ANNUAL REVIEW OF PROGRESS IN QUANTITATIVE NONDESTRUCTIVE EVALUATION: Incorporating the 10th International Conference on Barkhausen Noise and Micromagnetic Testing* (Vol. 1581, No. 1, pp. 1197-1204). AIP Publishing.

Slotwinski, J. A., Garboczi, E. J., & Hebenstreit, K. M. (2014). Porosity measurements and analysis for metal additive manufacturing process control. *Journal of research of the National Institute of Standards and Technology*, *119*, 494.

Smith, R. J., Hirsch, M., Patel, R., Li, W., Clare, A. T., & Sharples, S. D. (2016). Spatially resolved acoustic spectroscopy for selective laser melting. *Journal of Materials Processing Technology*, *236*, 93-102.

Song, B., Zhao, X., Li, S., Han, C., Wei, Q., Wen, S., ... & Shi, Y. (2015). Differences in microstructure and properties between selective laser melting and traditional manufacturing for fabrication of metal parts: A review. *Frontiers of Mechanical Engineering*, *10*(2), 111-125.

Song, C., Yang, Y., Liu, Y., Luo, Z., & Yu, J. K. (2015). Study on manufacturing of W-Cu alloy thin wall parts by selective laser melting. *The International Journal of Advanced Manufacturing Technology*, *78*(5-8), 885-893.

Spears, T. G., & Gold, S. A. (2016). In-process sensing in selective laser melting (SLM) additive manufacturing. *Integrating Materials and Manufacturing Innovation*, *5*(1), 1.

Strano, G., Hao, L., Everson, R. M., & Evans, K. E. (2013). Surface roughness analysis, modelling and prediction in selective laser melting. *Journal of Materials Processing Technology*, *213*(4), 589-597.

Tammas-Williams, S., Zhao, H., Léonard, F., Derguti, F., Todd, I., & Prangnell, P. B. (2015). XCT analysis of the influence of melt strategies on defect population in Ti–6Al–4V components manufactured by selective electron beam melting. *Materials Characterization*, *102*, 47-61.

Tang, H. P., Qian, M., Liu, N., Zhang, X. Z., Yang, G. Y., & Wang, J. (2015). Effect of powder reuse times on additive manufacturing of Ti-6Al-4V by selective electron beam melting. *Jom*, *67*(3), 555-563.

Tapia, G., & Elwany, A. (2014). A review on process monitoring and control in metal-based additive manufacturing. *Journal of Manufacturing Science and Engineering*, *136*(6), 060801.

Thijs, L., Verhaeghe, F., Craeghs, T., Van Humbeeck, J., & Kruth, J. P. (2010). A study of the microstructural evolution during selective laser melting of Ti–6Al–4V. *Acta Materialia*, *58*(9), 3303-3312.

Thomas, D. (2009). *The development of design rules for selective laser melting* (Doctoral dissertation, University of Wales).

Thombansen, U., Gatej, A., & Pereira, M. (2015). Process observation in fiber laser–based selective laser melting. *Optical Engineering*, *54*(1), 011008-011008.

Todorov, E., Spencer, R., Gleeson, S., Jamshidinia, M., & Kelly, S. M. (2014). *America Makes: National Additive Manufacturing Innovation Institute (NAMII) Project 1: Nondestructive Evaluation (NDE) of Complex Metallic Additive Manufactured (AM) Structures* (No. 55028GTH). EDISON WELDING INST INC COLUMBUS OH.

Tolochko, N.K., Mozzharov, S.E., Yadroitsev, I.A., Laoui, T., Froyen, L., Titov, V.I., Ignatiev, M.B., (2004) Balling processes during selective laser treatment of powders, Rapid Prototyping J. 10 (2), 78–87

Townsend, A., Senin, N., Blunt, L., Leach, R. K., & Taylor, J. S. (2016). Surface texture metrology for metal additive manufacturing: a review. *Precision Engineering 46, 34-47*.

Triantaphyllou, A., Giusca, C. L., Macaulay, G. D., Roerig, F., Hoebel, M., Leach, R. K., ... & Milne, K. A. (2015). Surface texture measurement for additive manufacturing. Surface Topography: Metrology and Properties, 3(2), 024002.

Van Belle, L., Vansteenkiste, G., & Boyer, J. C. (2013). Investigation of residual stresses induced during the selective laser melting process. In *Key Engineering Materials* (Vol. 554, pp. 1828-1834). Trans Tech Publications.

Van Elsen, M. (2007). *Complexity of Selective Laser Melting: a new optimisation approach* (Doctoral dissertation, Katholieke Universiteit Leuven).

Van Gestel, C. (2015). Study of physical phenomena of selective laser melting towards increased productivity. PhD Dissertation, Ecole Polytechnique Federale De Lausanne

Wang, C. M., Meng, X. X., Huang, W., Hu, X. Y., & Duan, A. Q. (2011). Role of side assisting gas on plasma and energy transmission during CO 2 laser welding. *Journal of Materials Processing Technology*, *211*(4), 668-674.

Wang, X., & Chou, K. Residual stress in metal parts produced by powder-bed additive manufacturing processes. In *proceedings of the 26th International solid freeform fabrication symposium* (pp. 1463-1474).

Wegner, A., & Witt, G. (2011, August). Process monitoring in laser sintering using thermal imaging. In *SFF Symposium, Austin, Texas, USA* (pp. 8-10).

Weingarten, C., Buchbinder, D., Pirch, N., Meiners, W., Wissenbach, K., & Poprawe, R. (2015). Formation and reduction of hydrogen porosity during selective laser melting of AlSi10Mg. *Journal of Materials Processing Technology*, *221*, 112-120.

Xia, M., Gu, D., Yu, G., Dai, D., Chen, H., & Shi, Q. (2016). Influence of hatch spacing on heat and mass transfer, thermodynamics and laser processability during additive manufacturing of Inconel 718 alloy. *International Journal of Machine Tools and Manufacture*, *109*, 147-157.

Yadroitsev, I., Gusarov, A., Yadroitsava, I., & Smurov, I. (2010). Single track formation in selective laser melting of metal powders. *Journal of Materials Processing Technology*, *210*(12), 1624-1631.

Yadroitsev, I., Krakhmalev, P., & Yadroitsava, I. (2014). Selective laser melting of Ti6Al4V alloy for biomedical applications: Temperature monitoring and microstructural evolution. *Journal of Alloys and Compounds*, *583*, 404-409.

Yasa, E., Deckers, J., Craeghs, T., Badrossamay, M., & Kruth, J. P. (2009, August). Investigation on occurrence of elevated edges in selective laser melting. In *International Solid Freeform Fabrication Symposium, Austin, TX, USA* (pp. 673-85).

Yasa, E., Kruth, J. P., & Deckers, J. (2011). Manufacturing by combining selective laser melting and selective laser erosion/laser re-melting. *CIRP Annals-Manufacturing Technology*, *60*(1), 263-266.

Zaeh, M. F., & Branner, G. (2010). Investigations on residual stresses and deformations in selective laser melting. *Production Engineering*, *4*(1), 35-45.

Zaeh, M. F., & Kahnert, M. (2009). The effect of scanning strategies on electron beam sintering. *Production Engineering*, *3*(3), 217-224.

Zäh, M. F., & Lutzmann, S. (2010). Modelling and simulation of electron beam melting. *Production Engineering*, *4*(1), 15-23.

Zeng, K. (2015). Optimization of support structures for selective laser melting. PhD Dissertation, University of Louisville

Zhang, B., Ziegert, J., Farahi, F., & Davies, A. (2016). In situ surface topography of laser powder bed fusion using fringe projection. *Additive Manufacturing*, *12*, 100-107.

Zhang, L. C., & Attar, H. (2015). Selective laser melting of titanium alloys and titanium matrix composites for biomedical applications: a review. *Advanced Engineering Materials*.

Zhao, C. X., Kwakernaak, C., Pan, Y., Richardson, I. M., Saldi, Z., Kenjeres, S., & Kleijn, C. R. (2010). The effect of oxygen on transitional Marangoni flow in laser spot welding. *Acta Materialia*, *58*(19), 6345-6357.

Zhong, M., Sun, H., Liu, W., Zhu, X., & He, J. (2005). Boundary liquation and interface cracking characterization in laser deposition of Inconel 738 on directionally solidified Ni-based superalloy. *Scripta materialia*, *53*(2), 159-164.

Zhou, X., Liu, X., Zhang, D., Shen, Z., Liu, W. (2015). Balling phenomena in selective laser melted tungsten. Journal of Materials Processing Technology 222, 33-42.

Zur Jacobsmühlen, J., Kleszczynski, S., Schneider, D., & Witt, G. (2013, May). High resolution imaging for inspection of laser beam melting systems. In *2013 IEEE International Instrumentation and Measurement Technology Conference (I2MTC)* (pp. 707-712). IEEE.

Zur Jacobsmühlen, J., Kleszczynski, S., Witt, G., & Merhof, D. (2013). Elevated Region Area Measurement for Quantitative Analysis Of Laser Beam Melting Process Stability. In *Instrum. Meas. Technol. Conf. I2MTC* (pp. 707-712).